AN ABSTRACT OF THE THESIS OF

Marco Keiluweit for the degree of Master of Science in Soil Science presented on February 1, 2010.

Title: Persistence of aromatic compounds in soils and sediments: A molecular perspective.

Abstract approved:

Markus Kleber

Abstract:

This thesis explores open questions regarding molecular forms and interactions of natural and synthetic aromatic compounds present in soils and sediments.

Plant biomass-derived black carbon (biochar) generated through incomplete natural and anthropogenic combustion processes is a major source of aromaticity in terrestrial ecosystems. Chapter one represents a detailed account of the variations in the chemical and physical nature of aromatic components of char black carbon.

Despite reports showing that aromatic compounds are degraded with relative ease, they are relatively persistent in subsurface environments. Chapter two highlights unique mechanisms of interaction (i.e., π-electron donor-acceptor interactions) by which aromatic molecules adsorb to mineral and organic phases. It is discussed how these interactions may contribute to the sequestration of aromatic compounds in soils and sediments.

Persistence of aromatic compounds in soils and sediments: A molecular perspective

by

Marco Keiluweit

A THESIS

submitted to

Oregon State University

In partial fulfillment of
the requirements for the
degree of

Master of Science

Presented February 1, 2010
Commencement June 2010

Master of Science thesis of Marco Keiluweit presented on February 1, 2010.

APPROVED:

Major Professor, representing Soil Science

Head of the Department of Crop and Soil Science

Dean of the Graduate School

I understand that my thesis will become part of the permanent collection of Oregon State University libraries. My signature below authorizes release of my thesis to any reader upon request.

Marco Keiluweit, Author

ACKNOWLEDGEMENTS

I am truly grateful to my major advisor, Markus Kleber, for his guidance and support and all the research opportunities I was provided with over the past two years. I greatly appreciated discussions with my committee members Jennifer A. Field and Mark G. Johnson. I also thank Fredrick G. Prahl and Margret A. Sparrow for assistance with pyrolysis procedures and elemental analysis. I would like to thank Peter S. Nico for his patience teaching me how to operate the synchrotron-based scanning transmission X-ray microscope, especially during late night shifts; special thanks to David Kilcoyne for providing "after hours" support to help us make the most of our time at ALS beamline 5.3.2. I am grateful to Elizabeth Brewer, Zachary Kayler, Lydia Zeglin, and Christophe Moni for their friendship, and for insightful and encouraging discussions. You made the painful lack of natural light in ALS much easier to endure!

I am deeply indebted to my family for active encouragement and constructive criticism alike. Thanks also to all my esteemed friends at home who were willing to put up with long distance phone calls to compensate for my continuous absence.

Finally, I would like to express sincere appreciation for financial support by the Heinrich-Böll Foundation and the Department of Crop and Soil Science at OSU.

CONTRIBUTION OF AUTHORS

All authors discussed the results and provided editorial comments on the manuscript entitled “Dynamic Molecular Structure of Plant Biomass-derived Black Carbon (Biochar)”. Keiluweit performed char production and characterization, integration of the results, and development of the manuscript. Peter S. Nico (Lawrence Berkeley National Laboratory) trained Keiluweit in STXM/NEXAFS analysis at beamline 5.3.2 of the Advanced Light Source (Berkeley, CA) and provided advise for data interpretation. Mark G. Johnson (U.S. Environmental Protection Agency, National Health and Environmental Effects Research Laboratory) advised Keiluweit on BET-N_2 surface area measurements and FT-IR analysis. Markus Kleber (Department of Crop and Soil Science, OSU) trained Keiluweit for X-ray diffraction measurements.

For the manuscript entitled “Molecular-level Interactions in Soils and Sediments: The Role of Aromatic π-Systems”, Keiluweit was responsible for literature research, synthesis of the the findings, and writing of the manuscript. Markus Kleber contributed to discussion and synthesis of the results and provided guidance in the writing process.

TABLE OF CONTENTS

LIST OF FIGURES

LIST OF APPENDIX TABLES

Table Page

1 General Introduction

Historically, natural and synthetic aromatic compounds have been perceived as "stable" or persistent in terrestrial environments due to the innate chemical stability of aromatic ring structures (*1, 2*). Recent approaches to conceptualize the dynamics of organic compounds in soils and sediments hold, however, that much more importance needs to be given to environmental controls on their stability. Therefore, this thesis explores if there are benefits to aromaticity other than its "stability" which promote the preservation of aromatic compounds in soils and sediments.

Aromatic moieties are ubiquitous in terrestrial environments and occur either as a fraction of natural organic matter (NOM) or as synthetic aromatic compounds. Commonly, we find phenolic compounds derived from plant lignins and tannins; aromatic compounds stemming from fungal melanin; and bacterial aromatic amino acids and steroid hormones (*1, 3-6*). As a consequence, alkaline extractions ("humic" substances) recover a substantial amount of aromatic components from NOM of soils and sediments. Based on ^{13}C NMR, Schnitzer (*7*) estimated that 20-60% of the total C in soil humic acids is aromatic in nature. In order to accurately assess the dynamic role of soils and sediments in the global C cycle, a better understanding of the mechanisms that preserve this seemingly "stable" pool of organic C is needed.

Synthetic aromatic compounds and materials have continuously been introduced in terrestrial environment since the early days of industrialization. Compounds as diverse as polycylic aromatic hydrocarbons, polychlorinated biphenyls, nitroaromatic compounds, and also nanoparticles such as fullerenes and carbon

nanotubes (*8-12*) are found. Given that all these compound classes are known or asserted to have negative impacts on environmental and human health, it is important to identify the mechanisms responsible for their persistence.

"Aromatic" is a quality that implies various features, properties, or behaviors to chemists with different backgrounds. The IUPAC (International Union of Pure and Applied Chemistry) definition reads *"cyclically conjugated molecular entities with a stability (due to the delocalization of mobile electrons) significantly greater than that of a hypothetical localized structure (e.g. Kekulé structure) possess aromatic character"*. It becomes clear that stability is intimately linked to aromaticity. In the case of aromatics, stability refers to kinetic stability (as opposed to thermodynamic stability). A molecule is kinetically stable if there are substantial activation barriers (e.g., high bonding energies within the structure) to all available reaction pathways. For instance, the activation energy for the conversion benzene (as a surrogate for aromatic molecules) to its elements is very large as a consequence of the delocalization of π-electrons (*13*).

With this definition in mind, the innate kinetic stability of natural and synthetic aromatic compounds has long served a satisfactory explanation for their persistence (*1, 2*). Particularly, the longevity of lignin and "humic" extracts in soils and sediments has been attributed to their aromatic nature (*1*). In soil science and related disciplines, the term "recalcitrance" is often used to describe kinetic stability or some other form of chemical stability inherent to specific compounds or biopolymers. However, the concept of recalcitrance as a dominant explanation for the persistence of NOM in terrestrial environments (*14*) has been increasingly challenged over the last

decade (*15-17*). Moreover, it is nicely illustrated in the contaminant literature that aromaticity (and, thus, kinetic stability) does not sufficiently protect aromatic compounds from biodegradation. For instance, both monoaromatic (e.g., alkylbenzenes and phenylalkanes) (*18*) and polycyclic aromatic hydrocarbons (*19*) are readily mineralized in aquatic systems. Both reductive and oxidative cleavage of aromatic ring structures are well-known processes carried out by microorganisms (*20*). Among environmental chemists it is therefore widely recognized that persistence of organic contaminants is not primarily dependent upon the chemical stability (or "recalcitrance") of the compound under consideration (*2*). Instead, environmental controls, such as interactions with matrix components in soils and sediments (e.g., mineral and organic phases), appear to be more relevant factors for the sequestration of specific organic compounds in soil and sediment environments (*2*).

However, if the natural kinetic stability of aromatic structures does not sufficiently explain the longevity of aromatic compounds, one may ask whether aromaticity provides other (i) protective qualities or (ii) functional properties, offering explanations for their persistence in soils and sediments. This overarching question served as a basis for two independent investigations into the effects of aromaticity reported in this thesis:

The first study discusses potential protective factors. The guiding hypothesis is that the prevalence and resistance of aromatic components of NOM is not only due to their chemical state, but also to their physical nature (e.g., crystallinity). The discovery of large amounts of black carbon (i.e., the solid residues of incomplete combustion: pyrogenic organic matter, char, charcoal and soot) in soils and sediments

worldwide disclosed an alternative source of aromatic C in terrestrial environments (*3, 21-23*). Black carbon (BC) is thought to predominantly consist of polycondensed aromatic sheets (graphene) (*21*). These graphene sheets are thought to be stacked, lending "graphitic" properties to BC. These crystal-like characteristic appear to offer an explanation for the longevity of aromatic C contained in the BC structure (*21*) . However, it was shown that some black carbon components structurally resemble decomposed NOM that is potentially more labile (*24*) and others find surprisingly short turnover times for black carbon in soils (*25*). The first chapter aims to resolve these conflicting reports and provides a robust characterization of the physical organization and chemical complexity of biomass-derived BC (or biochar) and, specifically, that of aromatic C.

The second study addresses the question as to whether aromaticity provides functional properties that may promote the preservation of aromatic compounds in soil and sediment matrices. Three independent observations suggest that aromatic moieties in natural and synthetic aromatic compounds are directly involved in surface interactions with mineral phases, potentially representing a mechanisms of protection: (i) Hydrophobic organic solutes with higher contents of aromatic C are preferentially adsorbed to clay minerals relative to hydrophilic solutes (*26, 27*); (ii) aromatic structures preferentially adsorb to surfaces when dissolved organic matter is reacted with minerals (*28-30*); and finally, (iii) spectro- and microscopic observations as well as results form soil fractionation procedures show that highly aromatic black carbon is consistently found in close association with minerals (*31, 32*). In addition, strong sorption of aromatic contaminants to mineral and organic matrix components has been

observed (*9, 33*). In these cases, strong affinities of aromatic contaminants for mineral and organic domains were mechanistically linked to the specific properties of aromatic π-systems. This second study is an attempt to offer a mechanistic explanation for these phenomena. Here the potential of aromatic π-systems to exert rather strong polar forces, and so influence the sorptive interactions of aromatic organic compounds with the organic and mineral inventory of terrestrial environments, is investigated.

2 Dynamic Molecular Structure of Plant Biomass-derived Black Carbon (Biochar)

by

Marco Keiluweit , Peter S. Nico, Mark G. Johnson, and Markus Kleber

Environmental Science & Technology

Vol. 44, No. 4, p. 1247–1253, 2010

Editor: Jerald Schnoor

University of Iowa, Iowa City

E-mail: est@uiowa.edu

Print Edition ISSN: 0013-936X

Web Edition ISSN: 1520-5851

2.1 Abstract

Char black carbon (BC), the solid residue of incomplete combustion, is continuously being added to soils and sediments due to natural vegetation fires, anthropogenic pollution, and new strategies for carbon sequestration ('biochar'). Here we present a molecular-level assessment of the physical organization and chemical complexity of biomass-derived chars and, specifically, that of aromatic carbon in char structures. BET-N_2 surface area, X-ray diffraction (XRD), synchrotron-based Near-edge X-ray Absorption Fine Structure (NEXAFS), and Fourier transform infrared (FT-IR) spectroscopy are used to show how two plant materials (wood and grass) undergo analogous, but quantitatively different physical-chemical transitions as charring temperature increases from 100 to 700°C. These changes suggest the existence of four distinct categories of char consisting of a unique mixture of chemical phases and physical states: (i) in transition chars the crystalline character of the precursor materials is preserved, (ii) in amorphous chars the heat-altered molecules and incipient aromatic polycondensates are randomly mixed, (iii) composite chars consist of poorly ordered graphene stacks embedded in amorphous phases, and (iv) turbostratic chars are dominated by disordered graphitic crystallites. The molecular variations among the different char categories translate into differences in their ability to persist in the environment and function as environmental sorbents.

2.2 Introduction

Black carbon (BC) is an important constituent of soils and sediments (*21, 34-36*). BC has received much attention for three reasons. First, there is a general lack of knowledge of the processes that lead to the loss of BC from soils and sediments which prevents a clear understanding of fluxes into and out of the Earth's slow cycling C pools (*36*). Second, the addition of synthetic BC ("biochar") in soils combined with bioenergy production has been suggested as a means to mitigate climate change (*37, 38*). Finally, BC in soils and sediments is recognized as an effective sorbent for potentially hazardous organic compounds (*35, 39*). Evidently, there is gathering interest in understanding the behavior of BC; precise information regarding the structure and properties of BC is needed. However, BC is not a well-defined chemical substance and encompasses C forms with varying degrees of aromaticity such as partly charred plant matter, char, soot, and graphite (*40*). This fact creates difficulties in quantifying BC concentrations in natural environments (*41*), it complicates the identification of biochars with properties beneficial to soils (*37*), and results in large variations in the sorptive potential of BC (*42*). Masiello (*36*) summarized the nature of the problem when she stated: "discrepancies between BC studies occur at least in part because of a lack of a common model of BC."

Biomass-derived char BC is defined as the solid residue of incomplete combustion. A widely accepted conceptual approach to represent the transient chemical properties of char BC is based on the gradual increase in aromaticity observed for the heat-induced transformation of plant biomass into char (*36, 43*). This concept is commonly referred to as the "combustion continuum" and assumes that,

with increasing charring temperature, plant biomass undergoes chemical transformations leading to the formation of aromatic ring structures, followed by a progressive condensation of smaller aromatic units into larger conjugated sheets (*21*). Recently, Knicker and co-workers (*24, 44*) conceptualized char BC created at a temperature of 350˚C and in the presence of O_2 as a heterogeneous mixture of thermally altered biomacromolecules with substantial substitution with O, H, and S and average cluster sizes of aromatic units smaller than six rings.

While Knicker et al. did not attempt to relate physical properties of their char BC to its molecular structure, the recent past has revealed indications of the occurrence of nonlinearities and phase transitions during the thermal decomposition of biomass, which can be explained only by relatively abrupt changes in physical properties of chars, namely crystallinity and porosity. For instance, N_2-accessible surface area (SA) of char BC exhibits a rapid increase at intermediate charring temperatures (*37, 42*). This is approximately the same temperature region where X-ray diffraction data (*45-47*) show a transition from low-density disordered C to the formation of turbostratic crystallites.

It thus appears critical for the prediction of fate and reactivity of char BC to relate the evolution of the chemical structure of chars created across a relevant temperature range to their physical properties. Consequently, the primary objective of this study is to integrate physical and chemical information into a comprehensive model for the physical nature of plant biomass-derived char. We test the hypothesis that physical transitions expressed by changes in SA along a representative charring temperature range are reflected in corresponding changes in crystal structure as

determined by X-ray diffraction. We further explore the extent to which physical phase transitions as observed by Paris et al. (*47*) are reflected in chemical changes, and test whether this information can be combined with chemical data to recognize specific categories of chars.

Plant biomass variability is considered by using lignin-rich Pine wood shavings (*Pinus ponderosa*) and lignin poor Tall fescue grass (*Festuca arundinacea*) starting materials for char production across a charring temperature range of 100 to 700˚C. The properties of the chars are characterized via elemental and gravimetric analysis, BET-N_2 SA measurements, and Fourier transform infrared spectroscopy. Synchrotron-based near-edge X-ray absorption fine structure spectroscopy at the carbon K absorption edge is employed to relate C speciation to the degree of structural order of carbonaceous matter.

2.3 Experimental Section

Char Production. Commercially available Ponderosa pine shavings were purchased through GEM Shavings in Auburn, WA. Tall Fescue was collected at the Oregon State University Hyslop Field Research Laboratory in Corvallis, OR. An automated plant-material grinder was used to obtain particle sizes of less than 1.5 mm for all materials. The ground plant materials were then air-dried at 40˚C for 48 hours to establish similar moisture contents. Leaving a head-space of about 100 mL, 280 g of ground plant material were placed in a heat-resistant Inconel 601 crucible (1500 mL; Metal Technology Inc., Albany, OR) and covered with a tight fitting Inconel lid to create oxygen-limiting conditions during the charring process. The plant biomass in the crucibles occupied 90% of the available space, leaving 150 mL headspace filled

with air. Given a O_2 content of air is approximately 20%, the charring process occurred in the presence of 30 mL O_2. With an average density of 1.309 g/L at 25˚C and a total biomass of 280 g, the O_2 availability amounts to ~8×10^{-5} g O_2 per g biomass.

The filled crucibles were placed in a 550 Series Fisher Scientific Isotemp muffle furnace (Fisher Scientific, Pittsburgh, PA) preheated to 100, 200, 300, 400, 500, 600 or 700˚C and charred at ambient pressure and atmosphere. The reported temperatures represent oven temperatures during preparation. The actual reaction temperature may differ from these values due to endothermic reactions during dehydration and exothermic reactions during pyrolysis. After charring for 1 hour, the closed crucible was immediately moved to a desiccator and allowed to cool. After weighing, the charred residue was transferred to airtight containers and stored in the dark. Char samples were milled to pass a <0.25 μm sieve (60 mesh) prior to further analyses. The char samples are hereafter referred to as WX00 (wood) and GX00 (grass) with "X" indicating the final charring temperature (100-700˚C). For comparison, fresh plant material (W000 and G000) receiving the same treatment was included in some analyses.

Char Characterization. All chars were subjected to proximate analysis according to the American Society for Testing and Materials (ASTM) D1762-84 (*48*) to determine volatile matter, fixed C, and ash contents. Essentially, in this analysis the char is heated in a covered crucible to 950 °C and held at this temperature for 6 min. The measured weight loss is defined as volatile matter (VM), and the residual solid is fixed C. Subsequently, the carbonized char is heated in an open crucible to 750 °C and

held at this temperature for 6 h. The material that remains in the crucible is defined to be ash. The reported char yield is the dry mass of char produced divided by the dry mass of the precursor (grass or wood) loaded into the crucible. The interested reader finds more information on proximate analyses and typical values for volatile matter and fixed carbon yields in Antal and Gondi (*49*).

Total carbon, nitrogen, and hydrogen of all wood and grass samples were measured on a Carlo Erba NA-1500 CNS analyzer (Carlo Erba Instruments, Milan, Italy). Removal of the H_2O trap allowed for the measurement of hydrogen. Samples were analyzed after being dried in air at 105˚C for 24 h. Total oxygen was calculated by mass balance.

BET-N_2 surface area. Specific surface areas of all char samples were obtained with N_2-adsorption measurements at liquid nitrogen temperature (77 K) using an NOVA 2200e surface area analyzer (Quantachrome Instrument Corp., Boynton Beach, FL) and ultra high purity (99.999%) gaseous nitrogen (Polar Cryogenics, Portland, OR). Degassing of the samples was performed in sample tubes at 60˚C under continuous N_2 gas flow for ~12h. The adequacy of degassing times was validated using the method described in the ASTM D4820-97 for black carbon N_2 adsorption measurements (*50*). Nitrogen adsorption was measured for a relative pressure range of 0.01-0.03 and specific surface areas were obtained from the most linear portion of the isotherm using a minimum of 10 data points. SAs were calculated based on the Brunauer-Emmett-Teller (BET) equation after Brunauer et al. (*51*) with a molecular surface area for N_2 of 0.162 nm^2. All N_2 measurements were performed in triplicate (N = 3).

FT-IR. Attenuated total reflectance Fourier transform infrared (ATR FT-IR) spectroscopy was performed using a Thermo Nicolet Nexus 470 FT-IR 6700 spectrophotometer equipped with a smart endurance single-bounce diamond ATR accessory (Thermo Fisher Scientific, Waltham, MA). Complete temperature series of grass and wood chars were scanned in the mid-infrared region from 4000 to 400 cm^{-1}. For each sample, 128 co-added spectra were recorded at a resolution of 2 cm^{-1} and processed using the OMNIC 2.1 software.

XRD. Ground char samples were back loaded into a 2.5 cm diameter circular cavity holder and run on a PANanalytical X'Pert Pro Instrument using Co-Kα radiation at 40 kV and 40 mA. Diffraction patterns were recorded by step scanning from 10-60° 2θ, with the sample spinning at 2 revolutions per second. For easier display, scans were subjected to a standardized background correction and noise reduction procedure using the X'pert High Score plus software and PlotIT 3.1.

NEXAFS. Near-edge X-ray Absorption Fine Structure (NEXAFS) spectra were collected from single particles of both wood and grass char temperature series using a synchrotron-based scanning transmission X-ray microscope (STXM) at the Advanced Light Source, Lawrence Berkeley National Laboratory, Beamline 5.3.2. Detailed operation principles of STXM/NEXAFS are published elsewhere (*52-54*) and will be described here only briefly.

Ground char particles were distributed on silicon nitride membranes with a thickness of 50 nm. Stacks of STXM images were acquired at the carbon K-edge (280-320 eV) for particles which allowed transmission of the X-ray beam. NEXAFS spectra were extracted from each stack for specific regions of the image. This imaging

technique provides the benefits of chemical mapping allowing for a detailed investigating of the chemical heterogeneity of char particles. Potential radiation damage of the char samples (*55*) was minimized by consistently avoiding dwell times of > 1.0 ms.

A minimum of three distinct particles with mean diameter of <20 μm were selected for each type of char. To avoid spectral distortion, spectra were extracted from particles or areas of the particles with an optical density of < 1.5. The extracted spectra were averaged over multiple regions and, if possible, the entire particle. The spectra for each particle were normalized to unity at the 310 eV position. Within temperature treatments, spectra were nearly congruent, allowing us to obtain a representative spectrum for each char sample by averaging over the spectra of the three particles. Peak assignment for FT-IR and NEXAFS (Table A-1 and A-2, respectively) including references are available in the Appendix.

2.4 Results and Discussion

Char Characterization. Table 1 displays the numerical results for proximate and elemental analyses and BET-N_2 SA measurements for wood and grass char samples generated at various charring temperatures. Yields begin to decline most rapidly at 200˚C for wood and at 300˚C for grass, and remain relatively stable above 400˚C. Final yields of grass char (~29%) are higher than those of wood char (~22%).

Table 1: Char and fixed-C yields, volatile matter (VM), ash contents, elemental compositions and ratios, and BET-N_2 surface area (N=3) of wood and grass chars prepared at various charring temperatures.

Sample	Yield	VM	Fixed C	Ash	C	N	H	O	H/C	O/C	BET SA[a]
	[wt %][b]								atomic ratio[b]		[m^2 g^{-1}]
W100	99.8	77.1	21.7	1.2	50.6	0.05	6.68	42.7	1.59	0.63	1.6±0.3
W200	95.9	77.1	21.4	1.5	50.9	0.04	6.95	42.2	1.64	0.62	2.3±0.1
W300	62.2	70.3	28.2	1.5	54.8	0.05	6.50	38.7	1.42	0.53	3.0±0.04
W400	35.3	36.4	62.2	1.4	74.1	0.06	4.95	20.9	0.80	0.21	28.7±1.5
W500	28.4	25.2	72.7	2.1	81.9	0.08	3.54	14.5	0.52	0.13	196±11
W600	23.9	11.1	85.2	3.7	89.0	0.06	2.99	8.0	0.40	0.07	392±11
W700	22.0	6.3	92.0	1.7	92.3	0.08	1.62	6.0	0.21	0.05	347±11
G100	99.9	69.6	23.5	6.9	48.6	0.64	7.25	44.1	1.81	0.69	1.8±0.4
G200	96.9	70.7	23.6	5.7	47.2	0.61	7.11	45.1	1.81	0.72	3.3±0.4
G300	75.8	54.4	36.2	9.4	59.7	1.02	6.64	32.7	1.34	0.41	4.5±0.6
G400	37.2	26.8	56.9	16.3	77.3	1.24	4.70	16.7	0.73	0.16	8.7±0.5
G500	31.4	20.3	64.3	15.4	82.2	1.09	3.32	13.4	0.48	0.12	50±0.4
G600	29.8	13.5	67.6	18.9	89.0	0.99	2.47	7.6	0.33	0.06	75±12
G700	28.8	9.1	71.6	19.3	94.2	0.70	1.53	3.6	0.20	0.03	139±11

[a] Shown are average values calculated from N replicate measurements ± standard deviations.

[b] Yields and fixed C, ash, and VM contents are on a water-free basis (dried at 105˚C). Elemental contents and atomic ratios are on water- and ash-free basis.

Volatile matter (VM) and fixed C contents gives a relative measure of the more labile and more stable components of chars, respectively. Volatile components of both wood and grass char decrease substantially between 400 and 600˚C. Fixed C values show a reverse trend in this temperature range. This corroborates observations by Schenkel (*56*) summarized in Antal and Gronli (*49*), who find a large increase of fixed C contents between 300 and 500˚C. Ash contents in wood char increase slightly at 400˚C and stabilize at ~4% at higher temperatures, whereas those of grass chars are generally higher and eventually stabilize at ~19%.

Relative elemental contents show the rapid loss of oxygen and hydrogen between 300 and 500˚C suggesting similar condensation reactions for wood and grass. When plotted in a typical van Krevelen diagram (Figure 1), the progressive decrease in the H/C and O/C atomic ratios with temperature follows the trajectory associated with dehydration reactions (*57*). N contents are relatively stable for wood chars but show a maximum (1.24%) at 400˚C, indicating the enrichment of N-containing compounds. Starting at 400 and 500˚C for wood and grass chars, respectively, a dramatic rise in SA is observed with increasing temperatures. Final values for wood char (347 m^2 g^{-1}) are significantly higher than those of grass char (140 m^2 g^{-1}). The falloff in SA observed for wood chars at the final temperatures is consistent with observations showing SA maxima at relatively high temperatures (500-900˚C) (*49*).

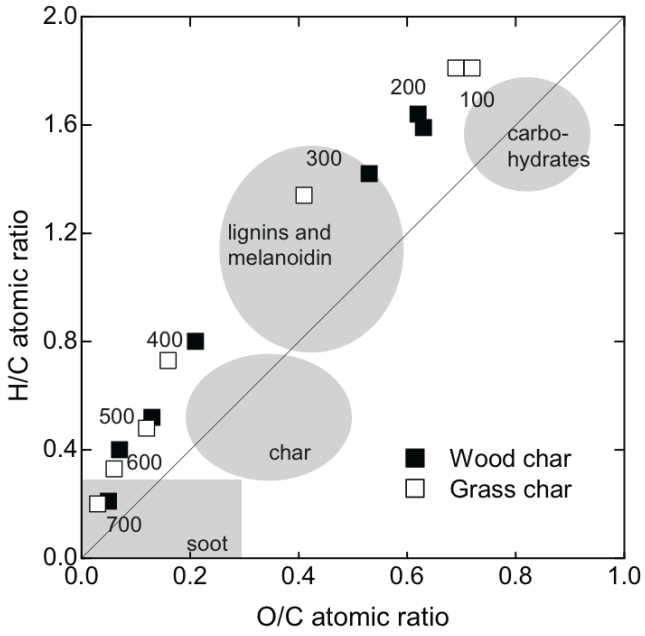

Figure 1: Van Krevelen plot of elemental ratios for wood and grass chars. Continuous line denotes the direction of dehydration reactions due the loss of H and O (2:1 ratio in H_2O) and grey shadings highlight approximate elemental ratios of unaltered biomacromolecules (lignin, melanoidin, and carbohydrates) and black carbon materials (char and soot) following Hammes et al. (*58*).

FT-IR. The evolution of FT-IR spectra of wood and grass chars as a function of charring temperature is shown in Fig. 2. The reader is referred to the Appendix for a more detailed discussion of these results. To summarize, (i) no FT-IR detectable chemical changes occur as plant material is heated to 100 and 200˚C. Spectra then show (ii) dehydration of cellulosic and ligneous components starting at 300˚C (3500-3200 cm^{-1}), (iii) presence lignin/cellulose-derived transformation products at 400˚C (multiple peaks 1600-700 cm^{-1}), and (iv) an increasing degree of condensation at charring temperatures of 500˚C and beyond (loss of intensity at 1650-1500 cm^{-1} relative to 885-752 cm^{-1}).

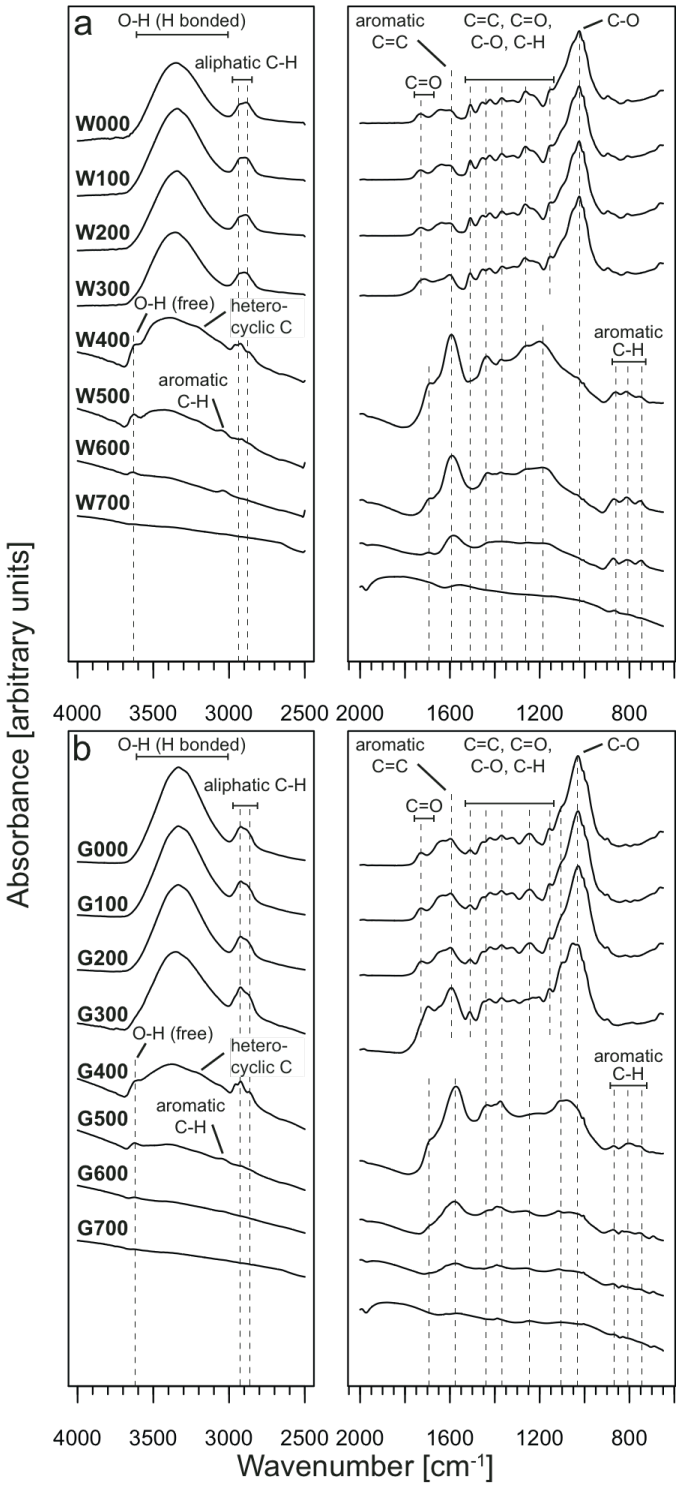

Figure 2: Stacked ATR FT-IR spectra of (a) wood and (b) grass char samples heated to temperatures ranging from 100 to 700˚C.

XRD. The X-ray diffraction patterns of the grass and wood chars are represented in Fig. 3, showing intensity of the diffracted beam as a function of the Bragg angle (˚2θ). Sharp, non-labeled peaks in grass chars indicate miscellaneous inorganic components. Although not discussed in detail, the greater prevalence of these peaks is consistent with the higher percentage of ash in the grass chars. Peak spacings of 0.60; 0.53; 0.404 and 0.259 nm are assigned to the hkl *101*, *110*, *200*, and *004* crystallographic planes of completely ordered (i.e., crystalline) regions of cellulose, respectively, assuming a monoclinic unit cell with c as the fiber axis (*59*). Spacings between 0.392 and 0.372 nm and between 0.209 and 0.207 nm are assigned to the hkl *002* and the overlapping *101*;*100* planes, respectively, of graphene sheets within turbostratic carbon crystallites (*45, 46*).

As the charring temperature increases from 100 to 300˚C, strong peaks from cellulose (i.e., 0.60, 0.53, 0.404, and 0.259 nm) progressively loose intensity and become broader (Fig. 3), indicating a gradual decrease in cellulose crystallinity. A complete loss of crystal structure in cellulose is indicated by the disappearance of the 0.60 and 0.53 nm signals and the coincidental shift of the 0.404 nm signal to higher angles in the 400˚C treatment (0.392 nm).

Further heating gives rise to broad peaks around 0.381 and 0.207 nm. The narrowing of these peaks with increasing temperature indicates developing atomic order in the increasingly carbonized plant material and is attributed to the formation and evolution of turbostratic crystallites. At advanced carbonization stages (i.e., temperatures > 400˚C), X-ray scattering has revealed progressive stacking of graphene sheets (*45, 47*). These small graphene packets are arranged in turbostratic disorder and

therefore referred to as turbostratic crystallites. Lateral growth of graphene planes is indicated by the increasing intensity of the *101*;*100* planes at 0.208-0.207 nm (*60*). Note that the 0.381 nm peak in the wood chars is narrower and shows much higher intensities than the signal in the respective grass chars (Fig. 3), indicating that wood chars are significantly more crystalline. Compared to XRD peaks of pure graphite (*61*), those of G700 and W700 are broad and featureless. The presented results are a further indication of the structural differences between chars consisting of turbostratic chrystallites and highly ordered graphite.

The XRD-data demonstrate that cellulose crystallinity of wood and grass chars is lost between 300 and 400˚C, while turbostratic crystallites evolve at charring temperatures above 400˚C. In addition to these two crystalline phases, X-ray scattering has revealed an intermediate, amorphous C stage within the narrow temperature interval 410-450˚C during the charring process of wood (*47*). Our data suggest such a disintegrated and entirely random C phase for wood and grass within a narrow temperature interval between 300 and 400˚C, where crystallinity stemming from both cellulosic components and turbostratic crystallites is at its minimum.

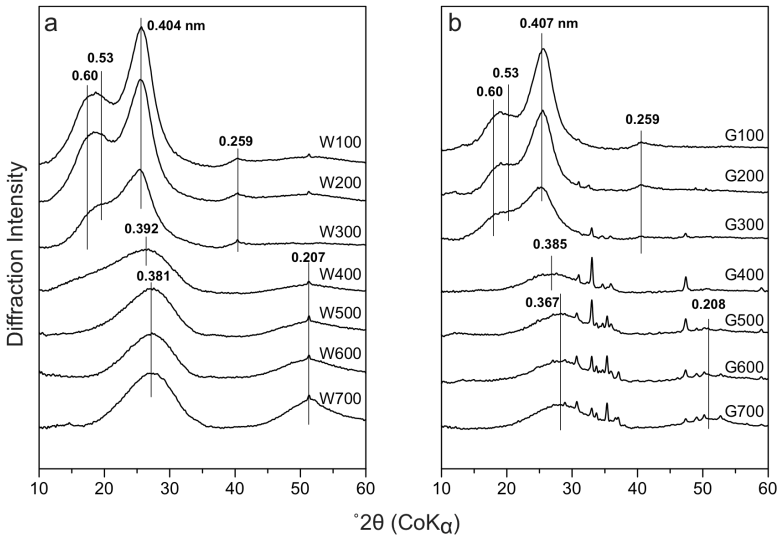

Figure 3: X-ray diffraction profiles (cobalt radiation) of (a) wood and (b) grass chars generated at temperatures ranging from 100 to 700˚C. Vertical lines indicate peak positions; associated numbers are d-spacings between crystallographic planes in nm. Sharp, non-labeled peaks are from inorganic components.

NEXAFS. Stacked C 1s NEXAFS spectra of each wood and grass char are displayed in Fig. 4. The large number of peaks observed at low temperatures (100-300˚C) demonstrates how the greater variety of C forms present in fresh plant material remains preserved. The 1s-π* C=C transition at 285.3 eV corresponding to H-, CH_3- or C-bonded aromatic C (*62*) is more prominent for wood than for grass, which can be ascribed to the higher lignin content of woody material. Further, lignin in coniferous wood (here Ponderosa Pine) is comprised of phenolic monomers derived from coniferyl alcohol, forming a peak at 287 eV which is prominent in the wood spectra (*55*). However, we also expect a contribution of the mixed 1s-3p/σ* resonance at this energy that correlates with aliphatic C-H. A second common feature associated with aromatic C is a broader band between 292 and 295 eV (1s-σ* resonance) (*63*). Spectra of grass chars show additional features in the intermediate region (286-287.5 eV). Here resonances of carbonyl groups (286.4 eV), aliphatic C-H and phenolic C-OH (287.1-287.3 eV) are located. At higher energies, carboxyl C-OOH (288.6 eV) and C-O (289.3 eV) of (hemi)cellulose and lignin are found (see peak assignments in Table A-2).

With intensity gains for the prominent bands in wood (285 and 287 eV) and almost all characteristic peaks in grass char at 300˚C, spectral features appear to be in a transitional state toward those observed at higher temperatures.

Charring at 400˚C results in a pronounced increase in aromatic C (1s-π* transition at 285 eV) and a drastic loss of other functional groups. The 1s-π* transition band slightly broadens, extending towards 284-285 and 286 eV. Absorption bands at this energy correspond to C=C π-transitions of molecules with low energy π* states

such as quinone-like components (*64, 65*). Concomitantly, almost all bands associated with O-containing and aliphatic groups in the intermediate region are lost.

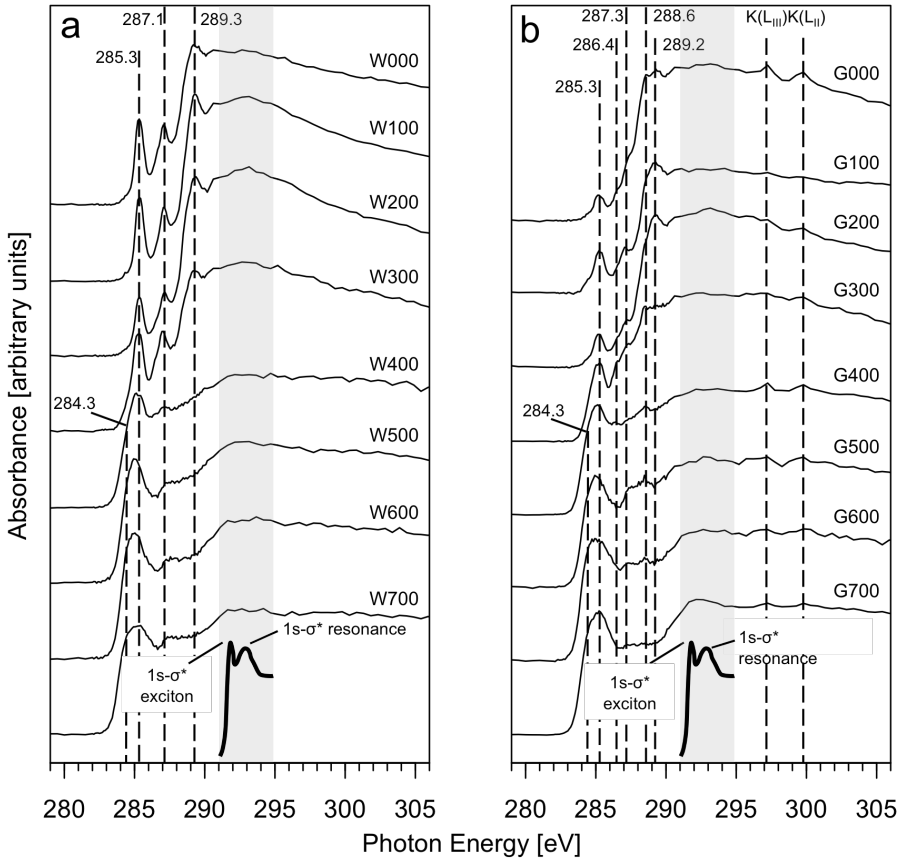

Figure 4: C NEXAFS spectra of (a) wood and (b) grass char temperature series including a non-charred sample of each. Individual spectra are shifted on the absorbance axis for better discrimination. The grey shaded area indicates the region in which 1s-σ* resonance and 1s-σ* exciton peak are located. The black line represents the idealized spectral features arising from 1s-σ* exciton and resonance characteristic of highly conjugated graphene sheets (adapted from . Additionally, absorption bands at 297.2 and 299 eV are attributed to potassium (K) L_{III} and L_{II} edges, respectively.

Increasing the charring temperature leads to the formation of a plateau between 286 and 288 eV. The gradual increase of the ratio of absorption at 285 eV (aromatic C) to that at 286-288 eV (aliphatic/oxygen-containing C) is an indication of the increasingly condensed nature of these chars. In pure graphite samples, this plateau is found at a 285 to 286-288 eV ratio of ~2.0 (*66*). In our work, the ratio for wood and grass chars are ~1.0 at 400˚C and, as the plateau gradually flattens, rises to ~1.5 at 700˚C. The remaining absorbance at 286.4 eV and 288.6 eV may be due to residual oxygenated functional groups (*67, 68*). However, this region has also been associated with "interlayer states" caused by poor alignment of graphene sheets (*66, 69*).

The notion that condensation takes place is further supported by the broad absorption band emerging at 500˚C between 291 and 295 eV. This signal is thought to arise from 1s-σ* C=C transitions (*70*) and has a possible contribution of the 1s-σ* exciton band (see below). The 1s-π* transitions at 285 eV are characteristic of aromatic double bonds, but lack information on the degree of condensation of these aromatic components. The 1s-σ* resonance, however, has been used to infer the degree of condensation and the long-range order of other carbonaceous materials (*65, 71*). Sharp 1s-σ* exciton peaks absorbing between 291 and 292 eV (see Fig. 4 for an idealized peak representation insert) are induced by long-range ordering of extensive polycondensed domains (see the Appendix for a brief discussion of 1s-σ* excitons). We observe evidence for such distinct features in spectra of chars produced at 600 and 700˚C (Fig. 3). Brandes et al. (*66*) used 1s-π* transitions in combination with 1s-σ* resonance and exciton features to propose a scheme to classify the crystallinity (i.e.,

the degree of structural order) of natural graphite samples. According to this scheme, well-ordered graphite features both distinct peaks at 285 eV and 292 eV as well as a distinctive 1s-σ* exciton peak. A missing or poorly expressed exciton peak, however, is thought to indicate the presence of smaller graphene sheets. Chars produced at 600 and 700˚C in this study would fall in the latter category, thus representing poorly crystalline materials.

NEXAFS spectra for chars reveal that (i) aromatic and quinonic compounds become prevalent while O-containing and aliphatic groups are lost at 400˚C, (ii) first evidence for condensation reactions is found at 500˚C, and (iii) chars produced at 600 and 700˚C are poorly crystalline in nature.

Specific Char Categories and their Components. FT-IR, XRD, and NEXAXS illustrate how chars derived from wood and grass biomass experience several phase transitions leading from microcrystalline cellulose over a largely amorphous intermediate phase towards the formation of turbostratic crystallites. They allow for the identification of four distinct categories of char (Figure 5).

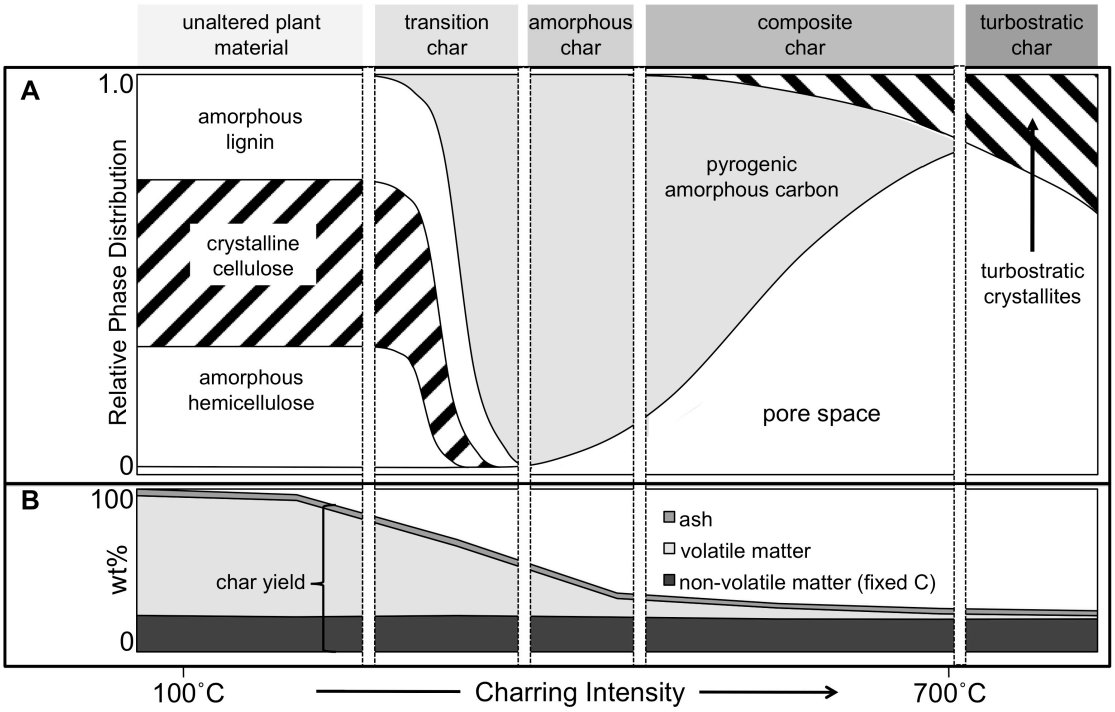

Figure 5: Dynamic molecular structure of plant biomass-derived black carbon (biochar) across a charring gradient and schematic representation of the four proposed char categories and their individual phases. (A) Physical and chemical characteristics of organic phases. Exact temperature ranges for each category are controlled by both charring conditions (i.e., temperature, duration, and atmosphere) and relative contents of plant biomass components (i.e., hemicellulose, cellulose, and lignin). (B) Char composition as inferred from gravimetric analysis. Yields, VM, fixed-C, and ash contents are averaged across wood and grass chars. Relative contributions above 700˚C are estimates.

Plant material: largely unaltered by thermal treatment

At initial charring stages, char yield and XRD-data indicate the loss of water and initial dehydration reactions of the wood and grass precursors. Overall, the native structure of the plant biopolymers (i.e., cellulose, hemicellulose, and lignin) remains preserved.

Transition chars: volatile dissociation products forming amorphous centers amidst a largely intact crystalline matrix

At the next charring stage, FT-IR spectra (loss of 1030 cm^{-1} peak) and lower H/C and O/C ratio clearly show that plant materials increasingly undergo dehydration and depolymerization of plant biopolymers, creating small volatile dissociation products. Greater signals of ketones, aldehyde, and carboxyl C observed in FT-IR spectra are indicative of depolymerization products derived from lignin (*72*) and cellulose (*73*). Volatile compounds such as anhydrosugars, pyrans, and furans are typical transformation products (*74-76*). Moreover, the stronger presence of phenols (NEXAFS absorbance at 285 eV and 287 eV) may form through secondary reactions of cellulose-derived intermediates (*75*). Despite the dissociation of such products, lignin sustains strong IR absorption (at 1510, 1440, and 1375 cm^{-1}) and XRD patterns illustrate that cellulose retains a notable portion of its crystallinity.

Amorphous char: an entirely amorphous mixture comprised of small, heat-resistant aliphatic and (hetero)aromatic elements

The sharp rise in aromatic C detected spectroscopically and the increasing growth of XRD reflections associated with condensation reactions are characteristic of

this charring stage. The absence of pronounced 1s-σ* features in the NEXAFS data indicates that there is not yet significant long range ordering as expected in the presence of larger condensed sheets. Instead, broad XRD signals present at 0.392-0.372 and 0.209-0.207 nm suggest the dominance of small aromatic units arranged in random order. In good agreement with the model proposed by Knicker et al. (*24, 44*) and studies of pyrolysis processes (*49, 74-76*), we observe (i) the formation of intermediates such as pyranones, anhydrosugars, phenols, quinones, pyrroles, and furans as well as small (poly)aromatic units, and (ii) the relative enrichment of stable aromatic lignin residues due to the loss of less heat-resistant material reflected in the dramatic decline in char yield, non-C atoms, and VM contents. In addition, substantial amounts of VM, along with aliphatic signals in NEXAFS and FT-IR spectra, suggest that not only cyclic and aromatic volatiles are retained. Almendros et al. (*77*) proposed that aliphatic components such as cutans and lipids are "fixed" in predominantly aromatic matrices, thereby resisting volatilization and degradation. The fact that crystalline cellulose is almost completely depolymerized combined with the evidence presented above suggest a disintegrated and randomly disordered C phase.

Composite char: turbostratic crystallites embedded in a low-density amorphous phase

A larger degree of condensation as reflected in FT-IR (out-of-plane vibrations) and NEXAFS spectra (285 to 286-288 eV ratio) and the formation of turbostratic crystallites as seen in the *002* XRD reflections are distinctive for chars formed upon further heating.

BET-N_2 SA values are well below the maximum achieved at higher temperatures, while gravimetric and elemental analyses indicate that some volatile

non-condensed components are retained in the char matrix. Bourke et al. (*61*) found that the lack of atomic pore space within the crystallite carbon layers as well as recondensation and trapping of VM in pores reduces the SA. Spectroscopic information presented in this study points specifically to the preservation of aromatic, aliphatic, and O-containing components, forming the amorphous matrix surrounding turbostratic crystallites.

Turbostratic char: nanoporous phase of turbostratic crystallites

At high temperatures, successive growth and increasing long-range order of the turbostratic crystallites are seen. Condensation proceeds as inferred from the more prominent 1s-σ* resonance band in NEXAFS spectra, whereas the appearance of the exciton feature, along with the evolution of the *002* XRD reflection, verifies the presence of increasingly crystalline structures. The dramatic rise in N_2-accessible SA at this charring stage is in part due to the lateral growth of graphene-like sheets at the expense of amorphous C (both aromatic and aliphatic) (*45*). The graphitic crystallites are denser than the original amorphous C forms, thus conversion of the former into the latter eventually leads to the formation of nanopores ($d < 2$ nm). Moreover, the fact that turbostratic chars are poorly crystalline in nature maintains a clear division between chars and natural or synthetic graphite. Bourke et al. (*61*) revealed the structural differences using XRD in conjunction with NMR and MALDI-TOF mass spectrometry. It is shown that the relatively high heteroatom content, SA, electrical conductivity, and the abundance of unpaired electrons in the structure unequivocally distinguish chars from graphite.

Fig. 5B summarizes the trends in char and fixed-C yield observed herein as well as those discussed in the review by Antal and Gronli (*49*). Collectively these studies report a rapid decrease in char yield and a relative increase in fixed-C yield at charring temperatures greater than ~250-300˚C followed by a stabilization in yields at charring temperatures greater than ~700˚C.

Comparison of Precursor Materials. FT-IR spectra and elemental ratios suggest that the breakdown of grass appears to begin at slightly lower temperatures than that of wood. Generally, heat-induced decomposition of hemicellulose and cellulose in biomass occurs rapidly at low temperatures (between 230-400˚C), whereas that of lignin happens over a broader temperature range (160-900˚C) (*78*). This suggests that the activation energy for heat-induced alteration of grass char is lower, presumably due to higher contents of thermally labile hemicelluloses, than for the more complex ligneous polymer structure of wood. The relative quantities of biopolymers in the native plant material thus determine the specific conditions under which biomass charring yields transition chars (Fig. 5).

The transition from amorphous C into ordered turbostratic crystallites is not only seen for wood chars, but also quite evident for grass chars. Consequently, the two-phase model by Kercher and Nagle (*45*) initially developed for wood chars may be applicable to various types of plant biomass. However, it is clear that higher yields of crystalline chars with larger SAs from wood can be achieved at lower temperatures than from grass biomass. This will be important for applications seeking to maximize the reactivity of chars as soil amendments (*37*).

Implications for degradability are probable and already have been suggested. Hamer et al. (*79*) showed that corn stover and rye char were mineralized more rapidly than wood char. Nguyen and Lehmann (*80*) reported that mineralization and oxidation decrease at higher temperatures for corn (grass) chars, whereas no such effect was observed for oak (wood) char.

Environmental Implications

Persistence in the Environment. The "paradox of refractory-labile BC" (*81*) refers to the lack of explanations for the large observed differences in residence time between seemingly refractory BC forms and other forms that appear to be more dynamic. Our investigation has revealed structural and chemical differences which make it plain that the persistence of BC in the environment depends to a great extend on its particular chemistry and physical structure. Attempts to rationalize observed variations in the chars' resistance to abiotic and biotic degradation (or "aging") (*57, 79*) will lead to more robust results when they are based on the multiphase model presented in Figure 5.

Chars as Environmental Sorbents. A clear distinction between the categories of chars and their various phases entering soils and sediments will aid the more accurate description of the sorption behavior of organic contaminants. Different types of char have different BC-water distribution coefficients (K_{BC}) (*35*). These variations are attributed to differences in SA and pore size distributions which are well-reflected in the proposed categories. Chen et al. (*42*) divides chars into a non-condensed partition (absorption) medium and carbonized phases that are viewed as a sorbent surface, but are indifferent toward the molecular properties of the non-condensed

phase. Our results show that mobile, non-condensed components may comprise both crystalline (i.e., native cellulose) and heat-altered amorphous components (i.e., lignin residues, aliphatics, and small (poly)aromatic units) which are expected to show dissimilar sorptive behavior.

Quantification in Environmental Systems. Despite substantial progress, different techniques yield widely varying BC "contents" for soils and sediments (*41*). These authors conclude that all quantification methods are selective, e.g., for amorphous wood char or more condensed wood chars. We suggest considering that the quantification protocols tested might be selective for one or more char categories. The reader is referred to the SI for a more detailed account of the environmental implications of the structural differences among the char categories.

We conclude with the suggestion that future research efforts need to recognize the existence of various categories of char BC with distinct (i) physical architecture and (ii) molecular compositions (Fig. 5). The unique combination of physical and chemical features in each category is likely to translate into widely differing dynamics and functions in soil and sediment environments. Future investigations of the effect of both charring conditions (e.g., charring duration and ramp rates) and biomass properties (e.g., other than wood and grass) on properties and yields of individual char categories will help to refine the presented classification scheme.

3 Molecular-level Interactions in Soils and Sediments: The Role of Aromatic π-Systems

by

Marco Keiluweit and Markus Kleber

Environmental Science & Technology

Vol. 43, No. 10, p. 3421–3429, 2009

Editor: Jerald Schnoor

University of Iowa, Iowa City

E-mail: est@uiowa.edu

Print Edition ISSN: 0013-936X

Web Edition ISSN: 1520-5851

3.1 Abstract

This review intends to deepen our understanding of mechanisms by which molecules with aromatic moieties attach to organic and mineral components of terrestrial environments. We present published evidence for the existence of specific, sorptive interactions of aromatic moieties with environmental sorbents. We find that aromatic pi-systems within organic compounds have the capacity to adsorb to minerals and organic soil and sediment components such as natural organic matter (NOM) and fire-derived black carbon (BC) through specific sorptive forces other than hydrophobic interactions. Polar interactions of aromatic pi-donor and -acceptor compounds show adsorption energies between 4 and 167 kJ mol^{-1}. Bonding strengths of cation-pi interactions and pi-pi electron donor-acceptor (EDA) interactions appear to be larger than H bonding strengths and comparable to inner- and outer-sphere complex formation. We conclude that, in analogy to polar and ionizable functional groups, components with aromatic pi-donor and -acceptor systems equip organic molecules with a substantial sorptive potential. This observation has important implications for the fate and transport of aromatic contaminants. The resulting sorptive interactions might also play a yet-overlooked functional role in the complex chain of processes which preserve NOM against decomposition.

3.2 Introduction

Aromatic structures are major components of natural and synthetic organic compounds in terrestrial environments. Scientific challenges such as the mitigation of climate change and remediation of hazardous industrial chemicals in soils and sediments require a thorough mechanistic understanding of the processes which determine the sorptive behavior of aromatic compounds.

In systems containing the polar solvent H_2O, bonding interactions of apolar aromatic ring structures have long been considered as restricted to energetically weak, non-specific, hydrophobic interactions (*82-85*). These interactions arise from enthalpy and entropy changes associated with water-water, aromatic compound-water, and sorbent-water interactions, as well as from Van der Waals (VdW) forces between aromatic rings and sorption sites.

Over the last decade, an increasing number of authors have suggested specific (i.e., directed) and energetically stronger adsorption mechanisms between aromatic π-systems of organic compounds and sorption sites at mineral surfaces, NOM, and BC. In particular, noncovalent electron donor-acceptor interactions of aromatic compounds with mineral surfaces have been proposed, including cation-π interactions (*86, 87*), n-π EDA interactions (*9, 88, 89*), and hydrogen-π interactions (*90*). Further, aromatic π-systems have been suggested to be involved in π-π EDA interactions, and polar-π interactions (*91, 92*) with NOM and BC. It appears that these interactions strongly affect the fate and transport of the most notorious aromatic organic contaminants such as polycyclic aromatic hydrocarbons (PAHs) and nitroaromatic compounds (NACs) in subsurface environments.

For this manuscript, however, we hypothesized that such interactions may be a hitherto overlooked factor for the sorptive protection of NOM by environmental sorbents, which has been increasingly recognized as a significant control on the persistence of NOM in soils and sediments (*30*). Based on ^{13}C nuclear magnetic resonance (NMR) data, Schnitzer (*93*) estimated that 20-60% of the total carbon in soil humic acids is aromatic. This led to the perception that high aromaticity is functionally responsible for the recalcitrance of humic substances (*93, 94*), that is, their resistance against decomposition. However, the concept of inherent recalcitrance as a major mechanism of NOM preservation (*14, 95*) recently has been challenged (*16*), raising the question whether adsorption mechanisms could be involved in the preservation of highly aromatic NOM. Finally, the discovery that many soils contain significant amounts of highly aromatic BC (*22, 96, 97*) led to yet-unresolved questions about the mechanisms that control their persistence in the environment (*36*), with sorption processes discussed as one possibility (*98*).

Consequently, the central objective of this work is to investigate published evidence to either confirm or reject the hypothesis that polar, noncovalent interactions of aromatic π-systems support adsorption of organic compounds to mineral and organic sorbents with energies stronger than non-specific, hydrophobic interactions (incl. VdW forces).

This review provides the reader with an assessment of what is known about polar interactions which have been reported to operate between aromatic π-systems and other soil and sediment components. We present information on mechanisms and bonding energies of such interactions for two important scenarios: (A) direct bonding

of aromatic rings to mineral surface sites, and (B) sorptive interactions between aromatic ring structures and organic environmental sorbents such as NOM and BC that may be free or mineral surface associated. Finally, we will address the question of whether polar interactions of aromatic π-systems provide energetic forces capable of influencing sorptive processes of organic compounds in soil and sediment environments.

3.3 Sorptive Behavior of Aromatic Structures

Hydrophobic effect. 'Hydrophobic interactions' or 'hydrophobic partitioning' largely determine the behavior of aromatic compounds without polar functional groups. The bonding enthalpies involved in hydrophobic interactions are considered negligible (*84*). Hydrophobic effects combine entropic forces, which drive hydrophobic organic compounds out of aqueous solution, with weak surface interactions resulting from VdW forces. The first step is homogeneous partitioning into hydrophobic domains. In the mineral phase, these are provided by neutral surface domains (*99, 100*) and hydrophobic macro-, meso-, micro-, and nano-pores (*101*). In close contact with hydrophobic regions, aromatic moieties are stabilized by VdW interactions. They include dipole-dipole, dipole-induced-dipole, and dispersive forces (*85, 99*), with the latter as the dominant contribution (*85, 102*). For high organic carbon environments, NOM acts as hydrophobic sorbent and aromatic structures dissolve, or partition, into this organic phase (*82, 85, 103*). Partitioning into organic phases or non-aqueous environments increases linearly with higher n-octanol-water partition coefficients, K_{ow}, and lower water solubility, S_w (*82*). High K_{ow} values of

aromatic compounds result from the molecular properties, such as the small dipole moment (i.e., low polarity), as well as the high polarizability and symmetry.

Specific Interactions. The presence of polarized or charged substituents on aromatic rings is thought to invoke interactions that are specific to the functional groups involved. Specific interactions include polar interactions such as H bonding as well as the formation of inner- and outer-sphere complexes with mineral surface sites or functional groups. Current understanding is that specific interactions of polar/ionized ring substituents are more likely to dominate adsorption at mineral surfaces than weak hydrophobic interactions of aromatic rings as the former involve much greater bonding enthalpies.

Electron Donor-Acceptor Interactions. The view that aromatic components of organic compounds play a passive, entropy-driven role in adsorption phenomena is challenged by the recognition of the existence of so-called electron donor acceptor interactions (or 'molecular' complexes). Originally introduced by Mulliken (*104-106*) and further discussed by Foster (*107, 108*) and the references cited therein, EDA interactions are based on the attractive forces between electron-rich (donors) and electron-deficient (acceptors) entities. In this case, electron-rich aromatic π-systems can act as π-donors, and electron-deficient π-systems as π-acceptors (*106, 108*). Regions of opposite charge attract the regions of charge associated with π-donor and -acceptor systems. A complete, quantitative description of π-EDA interactions is obtained by considering fundamental, intermolecular forces such as electrostatic, charge transfer, dispersive, and hydrophobic forces (*109*).

As a consequence of the charge associated with π-systems, EDA interactions occur between both π-donors (i.e., electron-rich π-systems) and π-acceptors (i.e., electron-deficient π-systems) with entities possessing the complementary property (electron-deficient or -rich, respectively). These entities include polarized and charged mineral surface sites, functional groups, and aromatic π-systems.

π-Donors and -Acceptors. The potential of aromatic π-donor and -acceptor compounds for EDA interactions become apparent when large quadrupole moments and substituent effects are considered (*108, 110, 111*).

Quadrupole moment. Benzene molecules have no net dipole moments, but they do have six local sp^2 $C^{\delta-}$-$H^{\delta+}$-bond dipoles (Fig. 6A). The quadrupole moment of benzene is viewed as the sum of these local dipoles between ring C atoms and substituents (*13, 112, 113*). A quadrupole can be illustrated by two molecular dipole moments aligned in a way ('tail-to-tail') that there is no net dipole (*112*) (Fig. 6A). Thus, uneven charge distributions between the π-electron clouds above and below the face of the ring (π-electron system) and the sp^2-hybridized C-atoms are created (*114*). Further addition of electron density to aromatic rings creates larger quadrupoles in which the electron-rich π-system can act as π-donor (Fig. 6B). Conversely, removal of electron density from aromatic structures can reverse the quadrupole moments, creating electron-deficient π-acceptors.

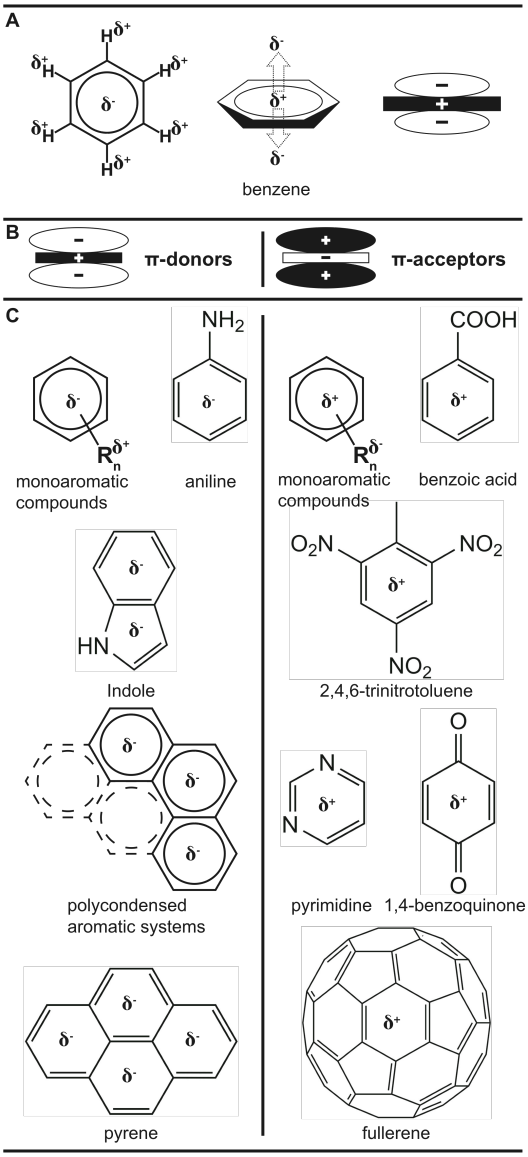

Figure 6: Aromatic π-donors and -acceptors. (A) Schematic representation of the quadrupole moment of benzene. 6 local dipoles (left) and the resulting two molecular 'tail-to-tail' dipoles (center). Schematic representation of the quadrupole moment, viewing the molecule edge-on (right). As a result of the molecular dipole moments, regions of positive (black) and negative (white) partial charge are created. Adapted from (*111, 112*). (B) Quadrupoles of aromatic π-donors and -acceptors. Note that benzene is a π-donor. (C) Effects of substituents on electron density in monoaromatic π-donor and -acceptor systems (above). Effects of heteroatoms on electron density in aromatic π-donor and -acceptor systems (center). Effects of additional fused rings on electron density of polyaromatic π-donor and -acceptor systems (below). In addition, illustrative examples for environmentally relevant aromatic π-donor and -acceptor compounds and functional components are presented. Electrostatic potential surfaces allow assessment of π-donor and -acceptor capacities for individual structures (*111, 113*).

Substituent effects. By changing the charge distribution within aromatic molecules, inductive and resonance effects of substituents affect the orientation of such quadrupoles. As shown in Figure 6C, a release of electron density into a monoaromatic system by one or more substituents that are less electron-withdrawing than hydrogen (designated $R^{\delta+}$) result in larger quadrupole moments. Such aromatic systems can be expected to act as π-donors (*85, 108, 115*). More electron-withdrawing substituents ($R^{\delta-}$), however, remove electron density from π-systems. This charge transfer results in quadrupoles which are opposite in sign, representing potent π-acceptors.

Common π-donors and -acceptors. Well-recognized aromatic π-donor and -acceptor systems are substituted monoaromatic π-systems, ring structures with heteroatoms, and associated fused rings (*108*) (Fig. 6C). Donor and acceptor strength increases with increasing polarizability of the compound or structure involved. For highly polarizable joint aromatic rings, e.g., PAHs and graphene-like polycondensed aromatic structures in black carbon, delocalizing resonance effects occur throughout the fused π-systems, resulting in strong permanent quadrupoles (*91*). Consequently, as the number of associated rings increases, the compounds become stronger π-donors. Other common types of π-acceptors are quinone-like structures, and nonclassical aromatic systems of fullerenes (C_{60}). N-heteroaromatic systems can function as both π-donors and -acceptors.

3.4 (A) Interactions at Mineral Surfaces

Cation-π interactions. The cation-π interaction is a noncovalent interaction between a cation and the planar surface of an aromatic π-donor system (Fig. 7). Electrostatically, it can be conceptualized as the interactions of a positively charged ion with the negative electrostatic potential surface of the ring (*113*). Dispersive and hydrophobic forces are thought to act in support of this type of association. The importance of these interactions, with bonding strengths comparable to cation-water complexes, has been widely recognized in biochemical processes (*114, 116, 117*). Binding energies for monovalent cations (e.g. Li^+, Na^+, K^+, and Rb^+) with benzene were reported to be as high as 167 kJ mol^{-1} in both gas-phase experiments (*116*) and theoretical computational studies (*118, 119*). Bonding strength increases with the size of the cyclic aromatic π-system (*119*) and the presence of electron-donating groups (*113*), that is, π-donor strength. Cations with low hydration energies generally promote cation-π interactions. Although lower energies may be expected for aqueous systems due to hydration of the cations, simulations have shown that cation-π interactions can result in significant bonding strengths (33 kJ mol^{-1} even when cations are surrounded by 3 water molecules) (*120*).

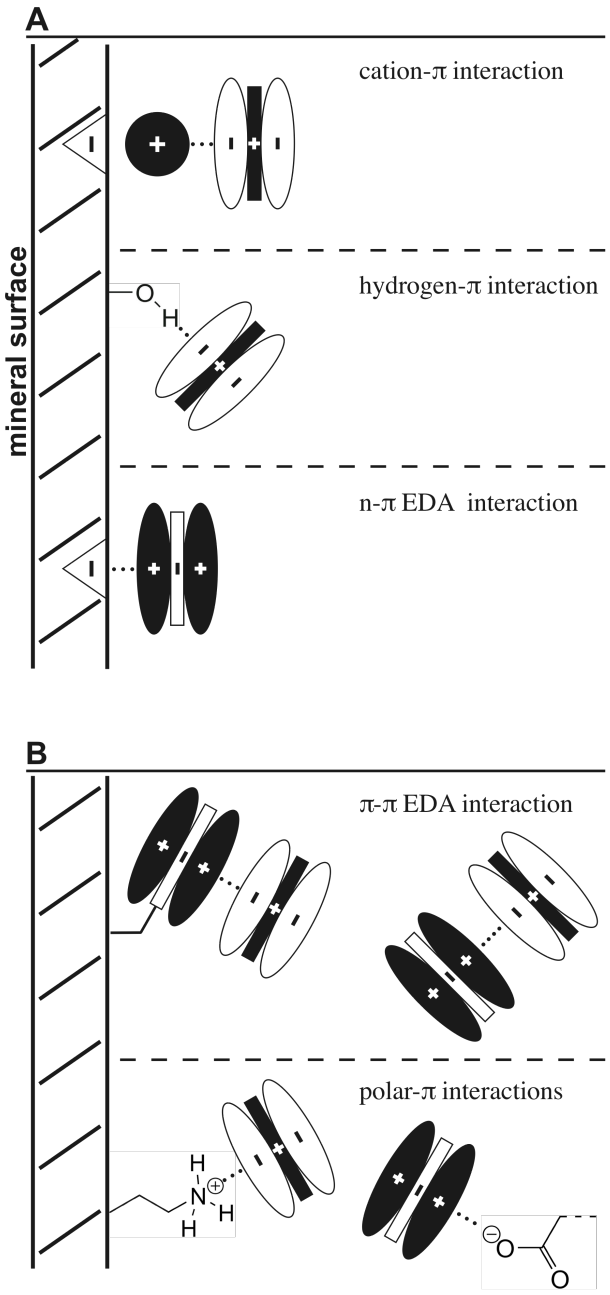

Figure 7: Schematic representation of aromatic interactions involving the π-system (indicated by ● ● ● -lines). Quadrupoles of π-donors and -acceptors presented as in Fig. 1. (A) Interactions with mineral surface sites. Exchangeable cations in cation–π interactions are drawn without potential hydration shell. (B) Intermolecular interactions. Polar-π interactions shown are organic cation-π (left) and n-π EDA/anion-π (right) interactions. Triangles represent permanent charge at mineral surface.

Direct cation-π bonding between PAHs and mineral surface cations was first hypothesized in attempts to model surface interactions of pyrene (*121*). According to contemporary theory, adsorption of PAHs to minerals is largely driven by hydrophobic interactions. However, Zhu et al. (*86*) made a contradicting observation when adsorption of phenanthrene to Ag^{+}-exchanged montmorillonite was 10 times stronger compared with 1,2,4,5-tetrachlorobenzene (TCB) sorption, despite very similar K_{ow} values. This observation was interpreted to indicate the existence of specific interactions between sorbate and mineral surface.

Zhu et al. (*86*) investigated this phenomenon under environmental (i.e., at least partly aqueous) conditions. Apparent distribution coefficients, log K_d, of different PAHs were higher to minerals (kaolinite, vermiculite, silica gel) saturated with weakly hydrated cations (Cs^{+}, Ba^{2+}, and especially Ag^{+}) than to minerals saturated with strongly hydrated cations. They also observed more upward-curving isotherms for PAHs (i.e., much higher affinities) with stronger π-donating properties, especially compared to the non-donor TCB. The strong effect of the type of cation and the π-donating properties of the solute suggested cation-π interactions.

In the attempt to verify cation-π interactions, ^{2}H NMR studies (*87*) were conducted to characterize the interactions between PAHs and a series of cations in aqueous solution. ^{2}H NMR relaxation times and calculations of molecular correlation times have been successfully used to investigate the sorption of deuteriated organic compounds with aromatic π-systems to geosorbents (*122, 123*), in particular cation-π interactions (*86, 87*). Quadrupole interactions of π-donor ^{2}H nuclei with the external magnetic field decreased more strongly upon adsorption to montmorillonite compared

with weak and non-donor molecules (toluene and tetrachloromethane, respectively). This was related to the stronger conformational adjustments necessary for π-donor molecules to undergo cation-π interactions observed in earlier studies. The overall binding energy increased in sequence $Ag^+ > Cs^+ > K^+ > Na^+$, Li^+, similarly matching the experimental results mentioned above. In the light of this evidence, cation-π interactions appeared the most tenable. Thus, the authors proposed that models for PAH-mineral interactions should combine non-specific effects of entropic forces with more specific cation-π interactions.

While the contributions cited above provide a solid platform to hypothesize that cation-π interactions occur, information on cation-π interactions in natural environments is missing. Hence, research should focus on the experimental substantiation of the mechanism with sorbent systems representative of terrestrial environments. Considering the high potential bonding strength, further attention should be given to the determination of bonding enthalpies.

Hydrogen-π interactions. Ringwald et al. (*90*) presented RAMAN and FTIR spectra that indicated hydrogen-π (H-π) interactions between the face of electron-rich π-systems of benzene and toluene and the H of silanol groups at dehydrated silica surfaces (Fig. 7). In the case of toluene, H-π bonding was preferred over H bonding between its methyl group and -OH surface groups. It was argued that significant bonding could arise from H-π interactions under dry and damp conditions, comparable in strength to benzene-water complexes (7.5 kJ mol^{-1}). For aqueous systems, competitive water adsorption would have to be considered.

n-π EDA interactions. Haderlein and Schwarzenbach (*9*) proposed that so-called n-π electron donor-acceptor interactions (n = non-bonding electrons at siloxane surfaces) contribute significantly to the retention of NACs such as trinitrotoluene, trinitrobenzene (TNB), and dinitro-*o*-cresol by phyllosilicates.

Due to the presence of electron-withdrawing nitro groups, the ring structures within NACs are excellent π-acceptors (*108*). The primary sorption sites are basal siloxane surfaces, which are shown to have both a large electronegative potential (*124, 125*) and, in agreement with Mulliken's EDA terminology (*106*), a significant n-donor capacity (*126*). The attractive forces between NACs (π-acceptors) and the non-bonding electrons (n-donors) were suggested to contribute significantly to the overall bonding energy (Fig. 7).

These additional specific interactions were inferred because entropy-driven processes did not adequately explain NAC adsorption behavior. Adsorption of NACs to phyllosilicates, as measured through surface area-normalized distribution coefficients (K_d), were up to 5 orders of magnitude larger than expected based on K_{ow} values (*89*). The calculated enthalpic contribution of hydrophobic interactions to the adsorption of NACs at Cs^+-exchanged kaolinite was 5 to 15 kJ mol^{-1} (*9*). The total adsorption enthalpies, however, were found to be 40 ± 5 kJ mol^{-1}. The difference of 25 to 40 kJ mol^{-1} was ascribed to the proposed specific n-π EDA interactions.

Experimental results of extensive studies were mostly consistent with this interaction (*9, 88, 89, 127, 128*). First, adsorption experiments and FTIR observations indicate a coplanar orientation of NACs and these siloxane surfaces (*88, 127, 129*). Second, relative affinities for various phyllosilicates are remarkably constant despite

substantially different structures and compositions of the mineral surfaces (*88, 89, 127, 129*). And finally, the presence of two or more nitro groups enhanced affinities substantially. As a general trend, greater adsorption was observed for NACs substituted with electron-withdrawing properties (e.g., $-NO_2$, -CHO, $-COCH_2$, and -CN), over such with electron-donating substituents (e.g., $-CH_3$, -OH, $-NH_3$) (*127*). Sorption for unsubstituted nitrobenzenes and organic compounds without nitrogroups is minimal ((*130*), and references cited therein).

The fact that NAC adsorption was strongly affected by the type of exchangeable cation, regardless of the type of phyllosilicate, gave rise to a substantial scientific debate. While adsorption to minerals exchanged with weakly hydrated cations (e.g., K^+, Cs^+, NH_4^+) was strong, strongly hydrated cations (e.g., Ca^{2+}, Mg^{2+}, Ba^{2+}) led to lower adsorption (*88, 89, 127, 129, 130*). Weissmahr et al. (*89*) argued that more extensive hydration shells would block siloxane surfaces for adsorbates and thereby hinder a suitable (i.e., coplanar) arrangement for n-π EDA interactions.

A different group of authors (*129-134*) suggested for smectites that exchangeable surface cations served as sorption sites for polar $-NO_2$ groups. Spectroscopic evidence for interactions between cations and $-NO_2$ groups of aromatic adsorbates were found in the literature (*135*), and were also obtained experimentally (*130, 131*). FTIR spectra showed shifts of peaks associated with the nitro groups upon adsorption to smectites exchanged with weakly hydrated cations (*129*). Furthermore, siloxane surfaces of smectites were shown to have 'hydrophobic nanosites' (*136*). Hydrophobic interactions with these sites are particularly favorable for weakly polar and nonpolar compounds (*137, 138*). Therefore, two simultaneous, additive

mechanisms were proposed for NAC adsorption (*131, 132*): (a) specific -NO_2-cation complexation, i.e., formation of inner- and outer-sphere complexes of -NO_2 and/or secondary substituents with exchangeable cations and their surrounding water molecules, respectively; and (b) partial or total dehydration of the NAC molecules and stabilizing dispersive forces upon coplanar arrangement at the underlying hydrophobic nanosites.

Most recently, the contribution of such hydrophobic interactions has been strongly emphasized over specific interactions (*132, 139*). This explanation appears plausible but it cannot account for the high adsorption values to highly charged and/or non-expandable clays (*9, 89*).

An *ab initio* quantum chemical study attributed the adsorption of TNB to 2:1 clay minerals to both electrostatic and dispersion forces between the face of the aromatic ring and the siloxane surface (*140*). The contributions to the calculated total binding energy (~40 kJ mol^{-1}) were ~15 and 25 kJ mol^{-1}, respectively. A more recent computational study investigated the relative contribution of 'specific electrostatic' and 'dispersion' forces to TNB adsorption process (*141*). The electrostatic contribution is thought to result from the overlap of the positive electrostatic potential observed for TNB and negative potentials of the siloxane surfaces. This is thought to initiate the accommodation of the TNB molecule on the surface. It accounted for half of the interaction energy, whereas the remaining dispersive contribution further stabilized the molecule in its position relative to the mineral surface.

In theory, the high bonding energies involved in cation complexation (up to 45 kJ mol^{-1} per NO_2-cation complex (*132*)) are most likely stronger than forces

involved in n-π EDA-interactions. Although conclusions drawn from *ab initio* studies should be generalized with care, both computational studies indicate strong electrostatic interactions between the face of the aromatic ring and the surface. The exact nature of these forces remains unclear, and the existence of n-π EDA interactions remains to be conclusively accepted or rejected.

As a final remark, the importance of quasicrystal dynamics phenomena for the adsorption of organic compounds to smectites should be noted. Generally, both cation-π and n–π EDA interactions are regulated by the amount and type of exchangeable cations present. In quasicrystalline smectites, in which some parts of the crystalline structures are ordered and some are nonperiodic, exchangeable cations are also thought to determine the ultrastructural organization in aqueous suspensions, thereby providing hydrophobic cavities for the sorption of NACs and PAHs (*142-145*). The complexity of the sorption system and the unclear role of exchangeable cations create experimental challenges when adsorption originating from cation-π or n-π EDA interactions is to be separated from such physical phenomena.

3.5 (B) Interactions with Free or Mineral Surface-associated Organic Matrix Components

π-π EDA interactions. π-π EDA interactions (or π-π stacking) are specific, noncovalent forces of attraction between π-donor and -acceptor molecules (*106, 108, 111, 146, 147*) (Fig. 7), and have been calculated to be as high as 17 kJ mol^{-1} (*111*).

Natural Organic Matter. Early studies suggesting π-π EDA interactions between π-acceptor components in humic fractions and π-donor herbicides are

summarized in Senesi and Miano (*148*). Since then, π-π EDA interactions have been proposed as relevant for the adsorption of π-donating contaminants (simple monoaromatic compounds, polyphenols, complex organic pesticides, and PAHs) to π-accepting sites in organic soil components. These are lignin (*149*), tannin (*150*), dissolved organic matter (*151*), and humic substances (*123, 152-158*). Most recently, π-π EDA interactions were inferred from experimental results presented in studies targeting the sorptive behavior of pesticides at the soil-water interface (*158, 159*).

Zhu et al. (*157*) and Wijnja et al. (*155*) systematically investigated the specific nature of the π-π EDA interactions between PAHs and model humic materials. According to their results, molecular π-π EDA complexes may be characterized by a parallel-planar but slightly offset orientation of the π-donor and -acceptor systems. This arrangement enables the two complimentary quadrupoles to interact, with electrostatic forces providing the majority of the contribution (*147*). To a lesser degree, attractive contributions such as VdW, charge-transfer, and solvent-driven interactions may be involved (*146*). These π-π interactions were established based on macroscopic and spectroscopic evidence, which demonstrated (i) effects of π-donor and -acceptor strength, suggesting π-π EDA interactions, and (ii) only minor contributions by hydrophobic effects.

Zhu et al. (*157*) and Wijnja et al. (*155*) found that interactions of π-donor molecules with π-accepting humic subunits were favored with increasing π-accepting ability of the subunits. Non-π-donors of similar hydrophobicity (in terms of K_{ow} and S_w) showed weaker interactions (*155, 158*). Inhibiting the potential for hydrophobic effects, by either reducing the water content of the solvent or raising acceptor polarity,

generally promoted the interactions (*152, 155*). Earlier studies showed that π-π EDA interactions are enhanced in apolar, nonaqueous solvents (*108*). Increasingly polar (i.e., less hydrophobic) acceptor molecules have reduced capacities to serve as a template for hydrophobic effects. PAH adsorption on humic acids was further found to increase with decreasing solution pH and higher % aromaticity of the sorbent (*123, 152, 156, 157*). Generally, the pH effect is attributed to the creation of hydrophobic domains in the sorbent upon protonation of functional groups. However, lower solution pH enhanced sorptive interactions with humic acids more for π-donors than for non-π-donor molecules (*157*). As the number of π-acceptor sites in the sorbent is also limited, it was argued instead that protonation of the functional groups may leave them more accessible for π-π interactions (*152, 157*). The two most recent studies (*156, 159*) point out, however, that π-π EDA interactions strongly require previous trapping of the aromatic sorbate in proximity to the π-acceptor domains via partitioning processes. Therefore, Xu et al. (*156*) suggested a 'host-guest interaction' (e.g. (*160, 161*)) as adsorption mechanism, in which molecules partition into hydrophobic domains, attach to them through dispersive forces, and then engage in π-π EDA interactions. For aqueous environmental systems, multiple bonding mechanisms are expected to operate simultaneously. The fact that host-guest interactions require several steps further complicates the estimation of actual binding strengths of π-π interactions.

The existence of π-π EDA complexes in these systems was supported by applying solution-phase ^{1}H NMR, ^{2}H NMR, UV/vis spectroscopy (*123, 155, 157*) and steady-state fluorescence spectroscopy (*152*). Most recently, ^{1}H HR-MAS STDD

NMR (*159*) and 2D diffusion ordered spectroscopy (*162*) were used. The parallel orientation of the two π-systems in π-π interactions leads to characteristic ring current effects on nuclei, which are known to result in detectable upfield shifts for protons (^{1}H NMR) (*163*). If charge-transfer occurs, that is, a certain degree of electron-transfer between donor and acceptor, a characteristic charge-transfer (CT) absorption band can be detected in the UV/vis signal (*108*). Zhu and co-workers (*155, 157*) found both upfield shifts and CT bands for PAHs interacting with humic subunits. They also demonstrated that upfield shifts are well correlated with the magnitude of interaction. The same relationship was established for monoaromatic π-acceptors interacting with humic materials (*162*). It was also shown that fluorescence quenching usually ascribed to hydrophobic effects occurred regardless of pH and even in apolar solvents (*152*). If tested, the shifts indicating π-π interactions were generally stronger with increasing π-donor and/or acceptor strength. The above-mentioned evidence establishes π-π EDA interactions as a significant binding force between compounds with aromatic π-donor or -acceptor systems and their functional counterparts present in NOM.

Black Carbon. Up to this point, we discussed π–π interactions between organic compounds and aromatic sites within NOM. However, strongly sorbing aromatic π-systems can be found in graphite-like black carbon (BC) (i.e., soot and char or charcoal). Graphite consists primarily of disordered stacks of graphene sheets, which tend to be highly polarizable (*35*). These fused aromatic rings may serve as both π-donor and -acceptors.

Surface sites close to polarized edge sites or defects of graphene sheets were reported to be electron-rich π-donors (*164, 165*). For the adsorption of π–acceptor

compounds such as quinones (*164*), phenolic, and nitroaromatic compounds (*165, 166*) to graphene units, VdW forces (hydrophobic effects), multilayer adsorption, H bonding, and intercalation as possible explanations for high sorption intensities were ruled out. Thus, Zhu and Pignatello (*165*) proposed π-π interactions, with Gibbs free energy contributions estimated to range from 12 to 25 kJ mol^{-1}.

π-accepting areas on either graphene subunits between the aforementioned donor sites (*165, 167*) or in soot (*168, 169*) were suggested to engage in π-π EDA interactions with a series of π-donors (benzene, toluene, PAHs). Zhu and Pignatello (*165*) estimated interaction energies to be weaker than those reported above, while *ab initio* calculations elsewhere obtained larger energies (*170*). In the latter case, it was shown that for π-donors adsorbing to graphene templates (coronene), energies increased with the number of rings from 43 kJ mol^{-1} (benzene) to 111 kJ mol^{-1} (benzo(g,h,i)perylene, six rings). Both increasing molecular size (*170*) and planarity (*171*) of the adsorbate were offered as explanations for this trend, and 'π-π VdW forces' (*170*) and "π-cloud overlap or π-π interactions" (ref. (6) in (*171*)) were proposed. Adsorption studies on carbon nanotubes (CNT) provide further insight into π-π EDA interactions at graphene templates. These rolled, cylindrical graphene sheets undergo π-π EDA interactions with π-acceptor moieties of tannic acids (*172*), as well as π-donors such as 2-naphthol and 1-naphthylamine (*92*). Furthermore, π-π EDA interactions of benzene structures with CNT structures enhance the adsorption of benzene derivatives (*173*), polymers, and surfactants (*174, 175*). Although the interaction energy of benzene with CNT is rather low (10 kJ mol^{-1}) (*176*), functional

groups strengthen this interaction by improving the π-donor and -acceptor capability relative to benzene (*173*).

BC model sorbents show high potentials for π-π EDA interactions which strongly affects the sorption of aromatic compounds. To what extent this may result in the preferential adsorption of aromatic pollutants or aromatic NOM to environmental BC represents an important future research area.

Self-stacking. Between aromatic structures without quadrupole moments of opposite sign, binding can occur via stacking interactions. Here π-π EDA interactions are not the predominant driving force. Stacking geometries for benzene are described in (*110*) and binding energies are reported to range from 4 to 30 kJ mol^{-1} (*111, 118, 177*).

Polar-π interactions. Aromatic π-systems can interact with positively polarized or charged organic moieties.

n-π EDA interactions. For this type of n-π EDA interaction, *organic* n-donors (n = non-binding electron) are considered. Non-bonding electrons of deprotonated, surface-associated carboxyl groups ($-COO^-$) found on bacterial membranes were proposed to serve as strong n-donors in n-π EDA interactions with π-accepting NACs (*178*). Likewise, deprotonated hydroxyl groups ($-O^-$) of substituted aromatics are reported to engage in n-π EDA interactions with π-acceptor sites at graphene surfaces (*92*). Similar interactions are recognized in supramolecular chemistry as 'anion-π interactions' or 'lone pair-π interactions' (*179*).

Hydrogen-π interactions. Amino and amide groups found in proteins, peptides, and amino acids, as well as thiols, represent polarized X-H structures

potentially serving as electron acceptors (*111, 180*). As the hydrogen points directly towards a π-donor system, these interactions are classified as weak H bonds rather than non-specific hydrophobic interactions (*180*) (Fig. 7). Electrostatic energy is mainly responsible for this attractive interaction (*181*). Meyer et al. (*111*) reported stabilization energies for amide-π interactions were 17 kJ mol^{-1}. Others showed that H-π interactions (NH-π) occur with energies between 6 and 7 kJ mol^{-1} (*181*).

Organic cation-π interactions. Cation-π interactions were proposed for the adsorption of PAHs to interlayers of montmorillonite saturated with alkyl-ammonium cations (*91*). ^{1}H NMR upfield shifts were observed, and it was shown that these were positively correlated with respective π-donor strengths of PAHs. Instead of H-π bonding with the intermediate H, direct cation-π interactions with the cationic centre (N^{+}) were suggested (Fig. 7). In model studies, calculated bonding energies for model $(CH_3)_4N^{+}$-benzene and NH_4^{+}-benzene complexes were 40 and 75 kJ mol^{-1}, respectively (*182, 183*). Considering the wide distribution of electron-donating and/or -accepting functional groups and organic cations in natural and synthetic organic materials, it is surprising that very few reports on such interactions in environmental systems exist.

3.6 Environmental Implications and Future Research Needs

Aromatic moieties with π-donor and -acceptor properties are ubiquitous in the organic materials belonging to the inventory of terrestrial environments. We were able to show that organic compounds carrying such aromatic moieties are able to engage in specific sorptive interactions with environmental sorbents. Such sorbents include phyllosilicate clay minerals, but also organic phases like NOM (e.g., humic

materials, tannins, and lignin) and BC model compounds, which may exhibit π-donor and -acceptor properties themselves.

For all these environmental sorbents, π-donor and -acceptor compounds consistently show higher sorption compared to non-π-donors/-acceptors, indicating a mechanistic significance of the extent to which they can be considered 'polarized'. This is reflected in the tendency of the large, permanent quadrupoles to force aromatic ring structures into certain arrangements with charged counterparts.

However, some studies reporting on such mechanisms convey a sense of ambiguity largely due to experimental and theoretical challenges inherently associated with detection, analysis, and quantification of noncovalent binding mechanisms (*110*). Moreover, the large numbers of different approaches (batch experiments, molecular simulations, or spectroscopic measurements) and sorption systems (choice of solvent, sorbate, and sorbent) used in the studies cited further complicate the identification of sorption mechanisms and assessments of their energetic contributions.

General trends for binding energies are nonetheless observed in the literature (Fig. 8): For cation-π and π-π EDA interactions, reported interaction energies are in some cases larger than those of H bonding (*184, 185*). Reported adsorption energies for hydrogen-π, n-π EDA, self-stacking, and polar-π interactions indicate comparable or weaker forces. It is important to note that reported energies are generally larger than those expected for VdW forces ($\leq$ 4 kJ mol^{-1}) typically associated with hydrophobic interactions.

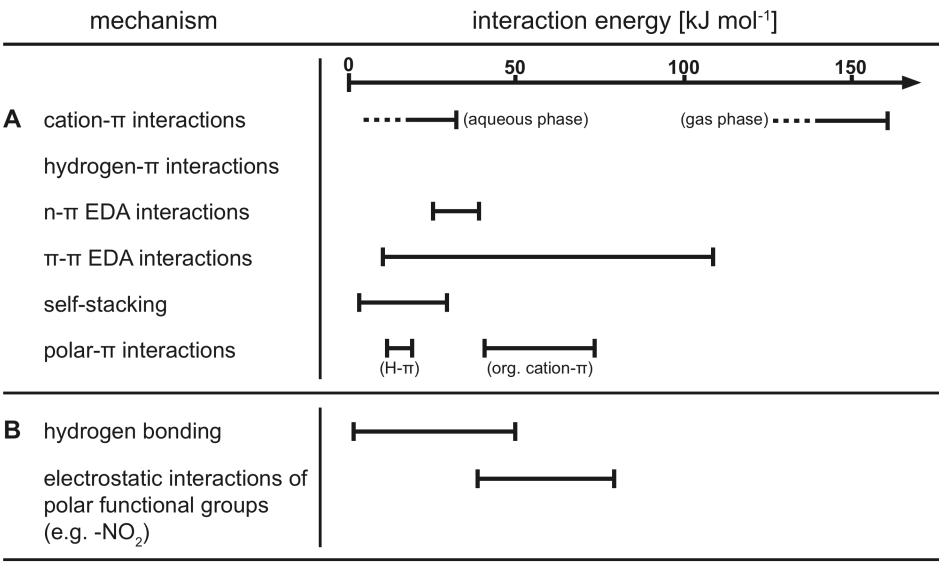

Figure 8: Potential interaction energies of important noncovalent adsorption mechanisms for aromatic moieties. (A) Polar interactions of aromatic π-systems. (B) Polar interactions of substituents (values for $-NO_2$ groups). The reader is refered to references in the text or in the original paper.

The presented evidence establishes polar molecular-level interactions of aromatic ring structures with environmental sorbents as an adsorption mechanism that affects fate and transport of organic contaminants. In complex natural environments, multiple sorption mechanisms are expected to operate simultaneously. For hydrophobic aromatic π-donor or -acceptor compounds without ionized functional groups (PAHs and other neutral organic compounds), these specific interactions appear to be the dominant force. For cases in which other mechanisms govern the sorption behavior of a specific compound, these interactions still have the potential to render the attachment of aromatic molecules to environmental sorbents more favorable.

The bonding energies are large enough to promote potential conformational changes within NOM and to facilitate its attachment to mineral surfaces. As proposed by Sutton and Sposito (*186*), relatively weak hydrophobic and H bonding interactions promote self-assembly of organic molecules. Polar interactions of aromatic rings are likely to stabilize the resulting supramolecular structures. Further investigation of this possibility might provide deeper insights into the still enigmatic structures of humic substances. In soils, NOM and clay minerals are generally aggregated in organo-mineral associations (*175, 187-189*). In some cases, NOM rich in aromatic carbon is shown to be intimately associated with mineral surfaces (*190, 191*). It is plausible that polar interactions of aromatic structures, in addition to hydrophobic and other binding forces, support the sorptive initiation of aggregate formation as proposed by Lehmann et al. (*189*). In turn, as these processes would affect the physical conformation of

NOM and the availability of sorption domains at mineral surfaces, implications for their function as potential sorbents for organic contaminants could arise (*192, 193*).

The extent to which specific non-covalent interactions of aromatic moieties in NOM contribute to its ability to persist in soils and sediments poses interesting challenges for future research. Another promising research area seems to be the sorption behavior of BC. The aromatic π-systems in black carbon are very receptive for EDA interactions and may be the key to an improved understanding of the sorptive capacity, persistence, and general environmental significance of this ubiquitous organic material.

4 Summary and Conclusions

This thesis highlighted specific properties and mechanisms by which aromatic compounds are preserved in soil and sediment environments.

The first chapter reveals that conflicting reports on the persistence of black carbon ("refractory-labile paradox") may indeed be a consequence of the variations in the molecular nature among different forms of black carbon. This study demonstrates the existence of four categories of plant biomass-derived char with distinct differences in their physical and chemical states. A recent complimentary study of the microbial and abiotic degradation of black carbon confirms the existence of individual phases (*194*). Here it is shown that only the poorly-crystalline, turbostratic C in chars can in fact be regarded as resistant against decomposition. Other, more labile char components (volatile matter) were mineralized quite rapidly.

The second chapter shows that sorptive forces exerted by aromatic π-systems are stronger than those expected for hydrophobic interactions. The strength of these forces, originating from electron donor-acceptor (EDA) interactions, suffices to explain observations for the preferential adsorption of aromatic compounds to organic and mineral phases in soils and sediments.

5 Bibliography

(1) Essington, M. E., *Soil and water chemistry: An integrative approach*. CRC Press LLC: Boca Raton, FA, 2004.

(2) Semple, K.; Morriss, A.; Paton, G., Bioavailability of hydrophobic organic contaminants in soils: fundamental concepts and techniques for analysis. *European Journal of Soil Science* **2003,** 54, 809-818.

(3) Haumaier, L.; Zech, W., Black carbon - possible source of highly aromatic components of soil humic acids. *Org. Geochem.* **1995,** 23(3), 191-196.

(4) Knicker, H.; Almendros, G.; GonzalezVila, F. J.; Ludemann, H. D.; Martin, F., C-13 and N-15 NMR analysis of some fungal melanins in comparison with soil organic matter. *Org. Geochem.* **1995,** 23(11-12), 1023-1028.

(5) Neale, P.; Escher, B.; Schäfer, A., pH dependence of steroid hormone—organic matter interactions at environmental concentrations *Sci. Total Environ.* **2008,** 407(3), 1164-1173.

(6) Preston, C. M., Applications of NMR to soil organic matter analysis: History and prospects. *Soil Sci.* **1996,** 161(3), 144-166.

(7) Schnitzer, M.; Kodoma, H.; Ripmeester, J. A., Determination of the aromaticity of humic substances by X-ray diffraction analysis. *Soil Sci. Soc. Am. J.* **1991,** 5(3), 745-750.

(8) Allen-King, R.; Grathwohl, P.; Ball, W., New modeling paradigms for the sorption of hydrophobic organic chemicals to heterogeneous carbonaceous matter in soils, sediments, and rocks. *Advances in Water Resources* **2002,** 25, 985–1016.

(9) Haderlein, S. B.; Schwarzenbach, R. P., Adsorption of substituted nitrobenzenes and nitrophenols to mineral surfaces. *Environmental Science & Technology* **1993,** 27(2), 316-326.

(10) Isaacson, C. W.; Kleber, M.; Field, J. A., Quantitative Analysis of Fullerene Nanomaterials in Environmental Systems: A Critical Review. *Environ. Sci. Technol.* **2009,** 43(17), 6463-6474.

(11) Lam, C. W.; James, J. T.; McCluskey, R.; Arepalli, S.; Hunter, R. L., A review of carbon nanotube toxicity and assessment of potential occupational and environmental health risks. *Critical Reviews in Toxicology* **2006,** 36(3), 189-217.

(12) Schlautman, M. A.; Morgan, J. J., Effects of aqueous chemistry on the binding of polycyclic aromatic hydrocarbons by dissolved humic materials. *Environ. Sci. Technol.* **1993,** 27(5), 961-969.

(13) Anslyn, E. V.; Dougherty, D. A., *Modern Physical Organic Chemistry*. University Science Books: Sausalito, Ca, 2006.

(14) Sollins, P.; Homann, P.; Caldwell, B. A., Stabilization and destabilization of soil organic matter: Mechanisms and controls. *Geoderma* **1996,** 74(1-2), 65-105.

(15) Baldock, J.; Oades, J.; Nelson, P.; Skene, T.; Golchin, A.; Clarke, P., Assessing the extent of decomposition of natural organic materials using solid-state C-13 NMR spectroscopy. *Australian Journal of Soil Research* **1997,** 35(5), 1061-1083.

(16) Marschner, B.; Brodowski, S.; Dreves, A.; Gleixner, G.; Gude, A.; Grootes, P. M.; Hamer, U.; Heim, A.; Jandl, G.; Ji, R.; Kaiser, K.; Kalbitz, K.; Kramer, C.; Leinweber, P.; Rethemeyer, J.; Schaeffer, A.; Schmidt, M. W. I.; Schwark, L.; Wiesenberg, G. L. B., How relevant is recalcitrance for the stabilization of organic matter in soils? *J. Plant Nutr. Soil Sci.* **2008,** 171(1), 91-110.

(17) Kleber, M., "Recalcitrant organic carbon, microbial decomposition, and carbon cycle-climate feedbacks. *Environ. Chem.* **2010,** in review.

(18) Pitter, P.; Chudoba, J., *Biodegradability of organic substances in the aquatic environment*. CRC Press LCC: Boca Raton, FA, 1990.

(19) Kanalay, R. A.; Harayama, S., Biodegradation of high-molecular-weight polycyclic aromatic hydrocarbons by bacteria. *J. Bacteriol.* **2000,** 182(8), 2059-2067.

(20) Madigan, M. T.; Martinko, J. M.; Dunlap, P. V.; Clark, D. P., *Brook biology of microorganisms*. Pearson Education, Inc.: San Francisco, CA, 2009.

(21) Preston, C. M.; Schmidt, M. W. I., Black (pyrogenic) carbon: a synthesis of current knowledge and uncertainties with special consideration of boreal regions. *Biogeosciences* **2006,** 3(4), 397-420.

(22) Rodionov, A.; Amelung, W.; Haumaier, L.; Urusevskaja, I.; Zech, W., Black carbon in the Zonal steppe soils of Russia. *J. Plant Nutr. Soil Sci.* **2006,** 169(3), 363-369.

(23) Skjemstad, J. O.; Clarke, P.; Taylor, J. A.; Oades, J. M.; McClure, S. G., The chemistry and nature of protected carbon in soil. *Aust J Soil Res* **1996,** 34(2), 251-271.

(24) Knicker, H., How does fire affect the nature and stability of soil organic nitrogen and carbon? A review. *Biogeochemistry* **2007,** 85(1), 91-118.

(25) Hammes, K.; Torn, M. S.; Lapenas, A. G.; Schmidt, M. W. I., Centennial black carbon turnover observed in a Russian steppe soil. In *Biogeosciences*, 2008; Vol. 5, pp 1339-1350.

(26) Guo, M. X.; Chorover, J., Transport and fractionation of dissolved organic matter in soil columns. *Soil Sci.* **2003,** 168(2), 108-118.

(27) Jardine, P. M.; Weber, N. L.; McCarthy, J. F., Mechanisms of dissolved organic-carbon adsorption on soil. *Soil Sci. Soc. Am. J.* **1989,** 53(5), 1378-1385.

(28) Balcke, G. U.; Kulikova, N. A.; Hesse, S.; Kopinke, F. D.; Perminova, I. V.; Frimmel, F. H., Adsorption of humic substances onto kaolin clay related to their structural features. *Soil Sci. Soc. Am. J.* **2002,** 66(6), 1805-1812.

(29) Chorover, J.; Amistadi, M. K., Reaction of forest floor organic matter at goethite, birnessite and smectite surfaces. *Geochim. Cosmochim. Acta* **2001,** 65(1), 95-109.

(30) Mikutta, R.; Mikutta, C.; Kalbitz, K.; Scheel, T.; Kaiser, K.; Jahn, R., Biodegradation of forest floor organic matter bound to minerals via different binding mechanisms. *Geochim. Cosmochim. Acta* **2007,** 71(10), 2569-2590.

(31) Brodowski, S.; Amelung, W.; Haumaier, L.; Abetz, C.; Zech, W., Morphological and chemical properties of black carbon in physical soil fractions as revealed by scanning electron microscopy and energy-dispersive X-ray spectroscopy. In *Geoderma*, 2005; Vol. 128, pp 116-129.

(32) Kaal, J.; Brodowski, S.; Baldock, J. A.; Nierop, K. G. J.; Martinez Cortizas, A., Characterisation of aged black carbon using pyrolysis-GC/MS, thermally assisted hydrolysis and methylation (THM), direct and cross-polarisation C-13 nuclear magnetic resonance (DP/CP NMR) and the benzenepolycarboxylic acid (BPCA) method. In *Organic Geochemistry*, 2008; Vol. 39, pp 1415-1426.

(33) Zhu, D.; Pignatello, J., Characterization of aromatic compound sorptive interactions with black carbon (charcoal) assisted by graphite as a model. *Environ. Sci. Technol.* **2005,** 39(7), 2033-2041.

(34) Kuhlbusch, T. A. J., Black carbon and the carbon cycle. *Science* **1996,** 280, 1903-1904.

(35) Koelmans, A. A.; Jonker, M. T. O.; Cornelissen, G.; Bucheli, T. D.; Van Noort, P. C. M.; Gustafsson, O., Black carbon: The reverse of its dark side. *Chemosphere* **2006,** 63(3), 365-377.

(36) Masiello, C. A., New directions in black carbon organic geochemistry. *Mar. Chem.* **2004,** 92(1-4), 201-213.

(37) Lehmann, J., Bio-energy in the black. *Front Ecol Environ* **2007,** 5(7), 381-387.

(38) Lehmann, J., A handful of carbon. *Nature* **2007,** 447(7141), 143-144.

(39) Loganathan, V. A.; Feng, Y.; Sheng, G. D.; Clement, T. P., Crop-residue-derived char influences sorption, desorption and bioavailability of atrazine in soils. *Soil Sci. Soc. Am. J.* **2009,** 73, 967-974.

(40) Seiler, W.; Crutzen, P. J., Estimates of gross and net fluxes of carbon between the biosphere and the atmosphere from biomass burning. *Climatic Change* **1980,** 2, 207-247.

(41) Hammes, K.; Schmidt, M. W. I.; Smernik, R. J.; Currie, L. A.; Ball, W. P.; Nguyen, T. H.; Louchouarn, P.; Houel, S.; Gustafsson, Ö.; Elmquist, M., Comparison of quantification methods to measure fire-derived (black/elemental) carbon in soils and sediments using reference materials from soil, water, sediment and the atmosphere. *Global Biogeochem. Cycles* **2007,** 21(3), GB3016, doi:10.1029/2006GB002914.

(42) Chen, B.; Zhou, D.; Zhu, L., Transitional adsorption and partition of nonpolar and polar aromatic contaminants by biochars of pine needles with different pyrolytic temperatures. *Environ. Sci. Technol.* **2008,** 42(14), 5137-5143.

(43) Hedges, J. I.; Eglinton, G.; Hatcher, P. G.; Kirchman, D. L.; Arnosti, C.; Derenne, S.; Evershed, R. P.; Kogel-Knabner, I.; de Leeuw, J. W.; Littke, R.; Michaelis, W.;

Rullkotter, J., The molecularly-uncharacterized component of nonliving organic matter in natural environments. *Org. Geochem.* **2000,** 31(10), 945-958.

(44) Knicker, H.; Hilscher, A.; Gonzalez-Vila, F. J.; Almendros, G., A new conceptual model for the structural properties of char produced during vegetation fires. *Org. Geochem.* **2008,** 39(8), 935-939.

(45) Kercher, A. K.; Nagle, D. C., Microstructural evolution during charcoal carbonization by X-ray diffraction analysis. *Carbon* **2003,** 41(1), 15-27.

(46) Kumar, M.; Gupta, R. C.; Sharma, T., X-ray diffraction studies of Acadia and Eucalyptus wood chars. *J. Mater. Sci.* **1993,** 28, 805-810.

(47) Paris, O.; Zollfrank, C.; Zickler, G. A., Decomposition and carbonisation of wood biopolymers - a microstructural study of softwood pyrolysis. *Carbon* **2005,** 43(1), 53-66.

(48) ASTM, *D1762-84 Standard Test Method for Chemical Analysis of Wood Charcoal*. Conshohocken, PA, 2007.

(49) Antal, M.; Gronli, M., The art, science, and technology of charcoal production. *Ind. Eng. Chem. Res.* **2003,** 42(8), 1619-1640.

(50) ASTM, *D4820-97 Standard Test Methods for Carbon Black—Surface Area by Multipoint B.E.T. Nitrogen Adsorption*. Conshohocken, PA, 1998.

(51) Brunauer, S.; Emmett, P. H.; Teller, E., Adsorption of gases in multimolecular layers. *J. Am. Chem. Soc.* **1938,** 60, 309-319.

(52) Braun, A., Carbon speciation in airborne particulate matter with C (1s) NEXAFS spectroscopy. *J. Environ. Monit.* **2005,** 7(11), 1059-1065.

(53) Kilcoyne, A. L. D.; Tyliszczak, T.; Steele, W. F.; Fakra, S.; Hitchcock, P.; Franck, K., Interferometer-controlled scanning transmission X-ray microscopes at the advanced light source. *J. Synchrotron Rad.* **2003,** 10, 125-136.

(54) Warwick, T.; Ade, H.; Kilcoyne, D.; Kritscher, M.; Tylisczcak, T.; Fakra, S.; Hitchcock, A.; Hitchcock, P.; Padmore, H., A new bend-magnet beamline for scanning transmission X-ray microscopy at the Advanced Light Source. *J. Synchrotron Rad.* **2002,** 9, 254-257.

(55) Cody, G.; Brandes, J.; Jacobsen, C.; Wirick, S., Soft X-ray induced chemical modification of polysaccharides in vascular plant cell walls. *J. Electron Spectrosc. Relat. Phenom.* **2009,** 170(1-3), 57-64.

(56) Schenkel, Y. Modelisation des flux massiques et energetiques dans la carbonisation du bois en four Cornue. Ph.D. Dissertation, Gembloux, Belgium, 1999.

(57) Baldock, J. A.; Smernik, R. J., Chemical composition and bioavailability of thermally altered Pinus resinosa (Red Pine) wood. *Org. Geochem.* **2002,** 33(9), 1093-1109.

(58) Hammes, K.; Smernik, R. J.; Skjemstad, J. O.; Schmidt, M. W. I., Characterisation and evaluation of reference materials for black carbon analysis using

elemental composition, colour, BET surface area and C-13 NMR spectroscopy. *Appl. Geochem.* **2008,** 23(8), 2113-2122.

(59) Koyama, M.; Helbert, W.; Imai, T.; Sugiyama, J.; Henrissat, B., Parallel-up structure evidences the molecular directionality during biosynthesis of bacterial cellulose. *Proc. Natl. Acad. Sci. U. S. A.* **1997,** 94(17), 9091-9095.

(60) Byrne, C.; Nagle, D., Carbonized wood monoliths - Characterization. *Carbon* **1997,** 35(2), 267-273.

(61) Bourke, J.; Manley-Harris, M.; Fushimi, C.; Dowaki, K.; Nunoura, T.; Antal, M. J., Do all carbonized charcoals have the same chemical structure? 2. A model of the chemical structure of carbonized charcoal. *Ind. Eng. Chem. Res.* **2007,** 46(18), 5954-5967.

(62) Urquhart, S. G.; Ade, H.; Rafailovich, M.; Sokolov, J. S.; Zhang, Y., Chemical and vibronic effects in the high-resolution near-edge X-ray absorption fine structure spectra of polystyrene isotopomers. *Chem. Phys. Lett.* **2000,** 322(5), 412-418.

(63) Cody, G.; Botto, R.; Ade, H.; Behal, S.; Disko, M.; al., e., Inner-shell spectroscopy and imaging of a subbituminous coal: In-situ analysis of organic and inorganic microstructure using C (1s)-, Ca (2p)-, and Cl (2s)-NEXAFS. *Energy Fuels* **1995,** 9, 525-533.

(64) Francis, J. T.; Hitchcock, A. P., Inner-shell spectroscopy of para-benzoquinone, hydroquinone, and phenol - distinguishing quinoid and benzenoid structures. *J. Phys. Chem.* **1992,** 96(16), 6598-6610.

(65) di Stasio, S.; Braun, A., Comparative NEXAFS study on soot obtained from an ethylene/air flame, a diesel engine, and graphite. *Energy Fuels* **2006,** 20(1), 187-194.

(66) Brandes, J. A.; Cody, G. D.; Rumble, D.; Haberstroh, P.; Wirick, S.; Gelinas, Y., Carbon K-edge XANES spectromicroscopy of natural graphite. *Carbon* **2008,** 46(11), 1424-1434.

(67) Cody, G. D.; Ade, H.; Wirick, S.; Mitchell, G. D.; Davis, A., Determination of chemical-structural changes in vitrinite accompanying luminescence alteration using C-NEXAFS analysis. *Org. Geochem.* **1998,** 28(7-8), 441-455.

(68) Hitchcock, A. P.; Urquhart, S. G.; Rightor, E. G., Inner-shell spectroscopy of benzaldehyde, terephthaladehyde, ethyl benzoate, terephthaloyl chloride, and phosgene - models for core excitation for poly(ethylene-terephthalate). *J. Phys. Chem.* **1992,** 96(22), 8736-8750.

(69) Fischer, D. A.; Wentzcovitch, R. M.; Carr, R. G.; Continenza, A.; Freeman, A. J., Graphitic interlayer states – a carbon-K near-edge X-ray-absorption fine-structure study. *Phys. Rev. B: Condens. Matter* **1991,** 44(3), 1427–1429.

(70) Stöhr, J., *NEXAFS spectroscopy*. Springer: New York, 1996.

(71) Banerjee, S.; Hemraj-Benny, T.; Balasubramanian, M.; Fischer, D. A.; Misewich, J. A.; Wong, S. S., Surface chemistry and structure of purified, ozonized, multiwalled carbon nanotubes probed by NEXAFS and vibrational spectroscopies. *ChemPhysChem* **2004,** 5(9), 1416-1422.

(72) Liu, Q.; Wang, S.; Zheng, Y.; Luo, Z.; Cen, K., Mechanism study of wood lignin pyrolysis by using TG-FTIR analysis. *J. Anal. Appl. Pyrolysis* **2008,** 82(1), 170-177.

(73) Reeves, J. B.; McCarty, G. W.; Rutherford, D. W.; Wershaw, R. L., Mid-infrared diffuse reflectance spectroscopic examination of charred pine wood, bark, cellulose, and lignin: Implications for the quantitative determination of charcoal in soils. *Appl. Spectrosc.* **2008,** 62(2), 182-189.

(74) Essig, M. G.; Richards, G. N.; Schenck, E. M., Mechanisms of formation of the major volatile products from the pyrolysis of cellulose. In *Cellulose and Wood Chemistry and Technology*, Schuerch, C., Ed. J. Wiley & Sons: New York, 1989.

(75) Pastorova, I.; Botto, R. E.; Arisz, P.; Boon, J., Cellulose char structure - a combined analytical PY-GC-MS, FTIR, and NMR-study. *Carbohydr. Res.* **1994,** 262(1), 27-47.

(76) Shafizadeh, F., Introduction to pyrolysis of biomass. *J. Anal. Appl. Pyrolysis* **1982,** 3(4), 283-305.

(77) Almendros, G.; Knicker, H.; Gonzalez-Vila, F. J., Rearrangement of carbon and nitrogen forms in peat after progressive thermal oxidation as determined by solid-state C-13 and N-15-NMR spectroscopy. *Org. Geochem.* **2003,** 34(11), 1559-1568.

(78) Yang, H.; Yan, R.; Chen, H.; Lee, D. H.; Zheng, C., Characteristics of hemicellulose, cellulose and lignin pyrolysis. *Fuel* **2007,** 86(12-13), 1781-1788

(79) Hamer, U.; Marschner, B.; Brodowski, S.; Amelung, W., Interactive priming of black carbon and glucose mineralisation. *Org. Geochem.* **2004,** 35(7), 823-830.

(80) Nguyen, B. T.; Lehmann, J., Black carbon decomposition under varying water regimes. *Org. Geochem.* **2009,** 40(8), 846-853.

(81) Czimczik, C. I.; Masiello, C. A., Controls on black carbon storage in soils. *Global Biogeochem. Cycles* **2007,** 21(3), GB3005, doi:10.1029/2006GB002798.

(82) Chiou, C. T.; Peters, L. J.; Freed, V. H., A physical concept of soil-water equilibria for nonionic organic compounds. *Science* **1979,** 206(4420), 831-832.

(83) Karickhoff, S. W., Organic pollutant sorption in aquatic systems. *Journal of Hydraulic Engineering* **1984,** 110(6), 707-735.

(84) Mader, B. T.; Goss, K.; Eisenreich, S. J., Sorption of nonionic, hydrophobic organic chemicals to mineral surfaces. *Environ. Sci. Technol.* **1997,** 31(4), 1079-1086.

(85) Schwarzenbach, R. P.; Gschwend, P. M.; Imboden, D. M., *Environmental Organic Chemistry*. Wiley-Interscience: New York, 2003.

(86) Zhu, D. Q.; Herbert, B. E.; Schlautman, M. A.; Carraway, E. R.; Hur, J., Cation-pi bonding: A new perspective on the sorption of polycyclic aromatic hydrocarbons to mineral surfaces. *J. Environ. Qual.* **2004,** 33(4), 1322-1330.

(87) Zhu, D. Q.; Herbert, B. E.; Schlautman, M. A.; Carraway, E. R., Characterization of cation-pi interactions in aqueous solution using deuterium nuclear magnetic resonance spectroscopy. *J. Environ. Qual.* **2004,** 33(1), 276-284.

(88) Haderlein, S. B.; Weissmahr, K. W.; Schwarzenbach, R. P., Specific adsorption of nitroaromatic explosives and pesticides to clay minerals. *Environ. Sci. Technol.* **1996,** 30(2), 612-622.

(89) Weissmahr, K. W.; Haderlein, S. B.; Schwarzenbach, R. P., Complex formation of soil minerals with nitroaromatic explosives and other pi-acceptors. *Soil Sci. Soc. Am. J.* **1998,** 62(2), 369-378.

(90) Ringwald, S. C.; Pemberton, J. E., Adsorption interactions of aromatics and heteroaromatics with hydrated and dehydrated silica surfaces by Raman and FTIR spectroscopies. *Environ. Sci. Technol.* **2000,** 32(2), 259-265.

(91) Qu, X.; Liu, P.; Zhu, D., Enhanced sorption of polycyclic aromatic hydrocarbons to tetra-alkyl ammonium modified smectites via cation-pi interactions. *Environ. Sci. Technol.* **2008,** 42(4), 1109-1116.

(92) Chen, W.; Duan, L.; Wang, L.; Zhu, D., Adsorption of hydroxyl- and amino-substituted aromatics to carbon manotubes. *Environ. Sci. Technol.* **2008,** 42(18), 6862-6868.

(93) Schnitzer, M., Soil organic matter - the next 75 years. *Soil Sci.* **1991,** 151(1), 41-58.

(94) Schnitzer, M.; Kodoma, H.; Ripmeester, J. A., Determination of the aromaticity of humic substances by X-Ray diffraction analysis. *Soil Sci. Soc. Am. J.* **1991,** 55(3), 745-750.

(95) Krull, E. S.; Baldock, J. A.; Skjemstad, J. O., Importance of mechanisms and processes of the stabilisation of soil organic matter for modelling carbon turnover. *Funct. Plant Biol.* **2003,** 30(2), 207-222.

(96) Haumaier, L.; Zech, W., Black Carbon - Possible source of highly aromatic components of soil humic acids. *Org. Geochem.* **1995,** 23(3), 191-196.

(97) Schmidt, M. W. I.; Noack, A. G., Black carbon in soils and sediments: analysis, distribution, implications, and current challenges. *Global Biogeochem. Cycles* **2000,** 14(3), 777-793.

(98) Hockaday, W. C.; Grannas, A. M.; Kim, S.; Hatcher, P. G., The transformation and mobility of charcoal in a fire-impacted watershed. *Geochim. Cosmochim. Acta* **2007,** 71(14), 3432-3445.

(99) Goss, K. U.; Schwarzenbach, R. P., Linear free energy relationships used to evaluate equilibrium partitioning of organic compounds. *Environ. Sci. Technol.* **2001,** 35(1), 1-9.

(100) Aggarwal, V.; Chien, Y.; Teppen, B. J., Molecular simulations to estimate thermodynamics for adsorption of polar organic solutes to montmorillonite. *Eur. J. Soil Sci.* **2007,** 58, 945-957.

(101) Mueller, S.; Totsche, K. U.; Koegel-Knabner, I., Sorption of polycyclic aromatic hydrocarbons to mineral surfaces. *Eur. J. Soil Sci.* **2007,** 58(4), 918-931.

(102) Su, Y. H.; Zhu, Y. G.; Sheng, G.; Chiou, C. T., Linear adsorption of nonionic organic compounds from water onto hydrophilic minerals: Silica and alumina. *Environ. Sci. Technol.* **2006,** 40(22), 6949-6954.

(103) Chiou, C. T., *Partition and adsorption of organic contaminants in environmental systems*. John Wiley & Sons: Hoboken, NJ, 2002.

(104) Mulliken, R. S., Molecular Compounds and their Spectra. II. *J. Am. Chem. Soc.* **1952,** 74, 811.

(105) Mulliken, R. S.; Person, W. B., Donor-Acceptor Complexes. *Annu. Rev. Phys. Chem.* **1962,** 13, 107-126.

(106) Mulliken, R. S. P., W. B., *Molecular Complexes: a Lecture and Reprint Volume*. Wiley-Interscience: New York, 1969.

(107) Foster, R.; Fyfe, C. A., Electron-donor-acceptor complex formation by compounds of biological interest. II. The association constants of various I,4-dinitrobenzene-phenothiazine drug complexes. *Journal of the Chemical Society B* **1966**, 926.

(108) Foster, R., *Organic Charge-Transfer Complexes*. Academic Press: New York, 1969.

(109) Morokuma, K., Why do molecules interact - Origin of electron donor-acceptor complexes, hydrogen bonding, and proton affinity. *Acc. Chem. Res.* **1977,** 10(8), 294-300.

(110) Muller-Dethlefs, K.; Hobza, P., Noncovalent interactions: A challenge for experiment and theory. *Chemical Reviews* **2000,** 100(1), 143-167.

(111) Meyer, E. A.; Castellano, R. K.; Diederich, F., Interactions with aromatic rings in chemical and biological recognition. *Angew. Chem.* **2003,** 42(11), 1210-1250.

(112) Dougherty, D. A., Cation-pi interactions in chemistry and biology: A new view of benzene, Phe, Tyr, and Trp. *Science* **1996,** 271(5246), 163-168.

(113) Mecozzi, S.; West, A. P.; Dougherty, D. A., Cation-pi interactions in aromatics of biological and medicinal interest: Electrostatic potential surfaces as a useful qualitative guide. *Proc. Natl. Acad. Sci. U. S. A.* **1996,** 93(20), 10566-10571.

(114) Ma, J. C.; Dougherty, D. A., The cation-π interaction. *Chem. Rev. (Washington, DC, U. S.)* **1997,** 97(5), 1303-1324.

(115) Carey, F. A. S., R.J., *Advanced organic chemistry: part A: structure and mechanisms*. Springer: New York, 2007.

(116) Kumpf, R. A.; Dougherty, D. A., A mechanism for ion selectivity in potassium channels: computational studies of cation-pi interactions. *Science* **1993,** 261(5129), 1708-1710.

(117) Gokel, G. W.; Barbour, L. J.; De Wall, S. L.; Meadows, E. S., Macrocyclic polyethers as probes to assess and understand alkali metal cation-π interactions. *Coord. Chem. Rev.* **2001,** 222(1), 127-154.

(118) Thomas, K. J.; Sunoj, R. B.; Chandrasekhar, J.; Ramamurthy, V., Cation-pi-interaction promoted aggregation of aromatic molecules and energy transfer within Y zeolites. *Langmuir* **2000,** 16(11), 4912-4921.

(119) Vijay, D.; Sastry, G. N., Exploring the size dependence of cyclic and acyclic pi-systems on cation-pi binding. *Phys. Chem. Chem. Phys.* **2008,** 10(4), 582-590.

(120) Xu, Y.; Shen, J.; Zhu, W.; Luo, X.; Chen, K. L.; Jiang, H., Influence of the water molecule on cation-π Interaction: ab initio second order Møller-Plesset perturbation theory (MP2) calculations. *J. Phys. Chem. B* **2005,** 109(12), 5945-5949.

(121) Kubicki, J. D.; Blake, C. A.; Apitz, S. E., Molecular models of benzene and selected polycyclic aromatic hydrocarbons in the aqueous and adsorbed states. *Environ. Toxicol. Chem.* **1999,** 18(8), 1656-1662.

(122) Zhu, D. Q.; Herbert, B. E.; Schlautman, M. A., Molecular-level investigation of monoaromatic compound sorption to suspended soil particles by deuterium nuclear magnetic resonance. *J. Environ. Qual.* **2003,** 32, 232-239.

(123) Nanny, M. A.; Maza, J. P., Noncovalent interactions between monoaromatic compounds and dissolved humic acids: A deuterium NMR T-1 relaxation study. *Environ. Sci. Technol.* **2001,** 35(2), 379-384.

(124) Gorb, L.; Gu, J.; Leszczynska, D.; Leszczynski, J., The interaction of nitrobenzene with the hydrate basal surface of montmorillonite: an ab initio study. *Phys. Chem. Chem. Phys.* **2000,** 2(21), 5007-5012.

(125) Michalkova, A.; Szymczak, J. J.; Leszczynski, J., Adsorption of 2,4-dinitrotoluene on dickite: The role of H-bonding. *Struct. Chem.* **2005,** 16(3), 325-337.

(126) Sposito, G., *The Chemistry of Soils*. Oxford: New York, 1984.

(127) Weissmahr, K. W.; Haderlein, S. B.; Schwarzenbach, R. P.; Hany, R.; Nuesch, R., In situ spectroscopic investigations of adsorption mechanisms of nitroaromatic compounds at clay minerals. *Environ. Sci. Technol.* **1997,** 31(1), 240-247.

(128) Weissmahr, K. W.; Hildenbrand, M.; Schwarzenbach, R. P.; Haderlein, S. B., Laboratory and field scale evaluation of geochemical controls on groundwater transport of nitroaromatic ammunition residues. *Environ. Sci. Technol.* **1999,** 33(15), 2593-2600.

(129) Boyd, S. A.; Sheng, G.; Teppen, B. J.; Johnston, C. T., Mechanisms for the adsorption of substituted nitrobenzenes by smectite clays. *Environ. Sci. Technol.* **2001,** 35(21), 4227-4234.

(130) Johnston, C. T.; De Oliveira, M. F.; Teppen, B. J.; Sheng, G. Y.; Boyd, S. A., Spectroscopic study of nitroaromatic-smectite sorption mechanisms. *Environ. Sci. Technol.* **2001,** 35(24), 4767-4772.

(131) Johnston, C. T.; Sheng, G.; Teppen, B. J.; Boyd, S. A.; De Oliveira, M. F.; Ce, Spectroscopic study of dinitrophenol herbicide sorption on smectite. *Environ. Sci. Technol.* **2002,** 36(23), 5067-5074.

(132) Li, H.; Teppen, B. J.; Johnston, C. T.; Boyd, S. A., Thermodynamics of nitroaromatic compound adsorption from water by smectite clay. *Environ. Sci. Technol.* **2004,** 38(20), 5433-5442.

(133) Li, H.; Teppen, B. J.; Laird, D. A.; Johnston, C. T.; Boyd, S. A., Geochemical modulation of pesticide sorption on smectite clay. *Environ. Sci. Technol.* **2004,** 38(20), 5393-5399.

(134) Sheng, G.; Johnston, C. T.; Teppen, B. J.; Boyd, S. A.; Lv, Adsorption of dinitrophenol herbicides from water by montmorillonites. *Clays Clay Miner.* **2002,** 50(1), 25-34.

(135) Saltzman, S.; Yariv, S., Infrared study of the sorption of phenol and p-nitrophenol by montmorillonite. *Soil Sci. Soc. Am. J.* **1975,** 39, 474-479.

(136) Jaynes, W. F.; Boyd, S. A., Hydrophobicity of siloxane surfaces in smectites as revealed by aromatic hydrocarbon adsorption from water. *Clays Clay Miner.* **1991,** 39(4), 428-436.

(137) Sheng, G. Y.; XU, S.; Boyd, S. A., Mechanism(s) controlling sorption of neutral organic contaminants by surfactant-derived and natural organic matter. *Environ. Sci. Technol.* **1996,** 30(5), 1553-1557.

(138) Laird, D. A.; Fleming, P. D., Mechanisms for adsorption of organic bases on hydrated smectite surfaces. *Environ. Toxicol. Chem.* **1999,** 18(8), 1668-1672.

(139) Roberts, M. G.; Li, H.; Teppen, B. J.; Boyd, S. A., Sorption of nitroaromatics by ammonium- and organic ammonium-exchanged smectite: Shifts from adsorption/complexation to a partition-dominated process. *Clays Clay Miner.* **2006,** 54, 426-434.

(140) Pelmenschikov, A.; Leszczynski, J., Adsorption of 1,3,5-trinitrobenzene on the siloxane sites of clay minerals: ab initio calculations of molecular models. *J. Phys. Chem. B* **1999,** 103(33), 6886–6890.

(141) Gorb, L.; Lutchyn, R.; Zub, Y.; Leszczynska, D., The origin of the interaction of 1, 3, 5-trinitrobenzene with siloxane surface of clay minerals. *Journal of Molecular Structure: THEOCHEM* **2006,** 766(2-3), 151-157.

(142) Chatterjee, R.; Laird, D. A.; Thompson, M. L., Interactions among K+-Ca2+ exchange, sorption of m-dinitrobenzene, and smectite quasicrystal dynamics. *Environ. Sci. Technol.* **2008,** 42(24), 9099-9103.

(143) Hundal, L. S.; Thompson, M. L.; Laird, D. A.; Carmo, A. M., Sorption of phenanthrene by reference smectites. *Environ. Sci. Technol.* **2001,** 35(17), 3456-3461.

(144) Li, H.; Pereira, T. R.; Teppen, B. J.; Laird, D. A.; Johnston, C. T.; Boyd, S. A., Ionic strength-induced formation of smectite quasicrystals enhances nitroaromatic compound sorption. *Environ. Sci. Technol.* **2007,** 41(4), 1251-1256.

(145) Pereira, T. R.; Laird, D. A.; Thompson, M. L.; Johnston, C. T., Role of smectite quasicrystal dynamics in adsorption of dinitrophenol. *Soil Sci. Soc. Am. J.* **2008,** 72, 347-354.

(146) Hunter, C. A.; Lawson, K. R.; Perkins, J.; Urch, C. J., Aromatic interactions. *Journal of Chemical Society: Perkin Transactions 2* **2001**, 651-669.

(147) Hunter, C. A.; Sanders, J. K. M., The nature of. pi.-. pi. interactions. *J. Am. Chem. Soc.* **1990,** 112, 5525–5534.

(148) Senesi, N.; Miano, T. M., The role of abiotic interactions with humic substances on the environmental impact of organic pollutants. In *Environmental Impact of Soil Component Interactions*, Huang, P. M.; Bollag, J. M.; McGill, W. B., Eds. 1995; p 309.

(149) Wang, X.; Cook, R.; Tao, S.; Xing, B., Sorption of organic contaminants by biopolymers: role of polarity, structure and domain spatial arrangement. *Chemosphere* **2007,** 66, 1476–1484.

(150) Li, H. T.; Hao, Y. C.; Xu, M. C.; Shi, Z. Q.; He, B. L., Thermodynamics aspect of tannin sorption on polymeric adsorbents. *Polymer* **2004,** 45(1), 181-188.

(151) Wershaw, R. L., Molecular aggregation of humic substances. *Soil Sci.* **1999,** 164(11), 803-813.

(152) Gadad, P.; Lei, H.; Nanny, M. A., Characterization of noncovalent interactions between 6-propionyl-2-dimethylaminonaphthalene (PRODAN) and dissolved fulvic and hurnic acids. *Water Res.* **2007,** 41(19), 4488-4496.

(153) Senesi, N., Binding mechanisms of pesticides to soil humic substances. *Sci. Total Environ.* **1992,** 123, 63-76.

(154) Senesi, N.; Dorazio, V. D.; Miano, T. M., Adsorption mechanisms of s-triazine and bipyridylium herbicides on humic acids from hop field soils. *Geoderma* **1995,** 66(3-4), 273-283.

(155) Wijnja, H.; Pignatello, J. J.; Malekani, K., Formation of pi-pi complexes between phenanthrene and model pi-acceptor humic subunits. *J. Environ. Qual.* **2004,** 33(1), 265-275.

(156) Xu, D. P.; Zhu, S. Q.; Chen, H.; Li, F. S., Structural characterization of humic acids isolated from typical soils in China and their adsorption characteristics to phenanthrene. *Colloids Surf., A* **2006,** 276(1-3), 1-7.

(157) Zhu, D. Q.; Hyun, S. H.; Pignatello, J. J.; Lee, L. S.; Hk, Evidence for pi-pi electron donor-acceptor interactions between pi-donor aromatic compounds and pi-acceptor sites in soil organic matter through pH effects on sorption. *Environ. Sci. Technol.* **2004,** 38(16), 4361-4368.

(158) Liu, P.; Zhu, D. Q.; Zhang, H.; Shi, X.; Sun, H.; Dang, F., Sorption of polar and nonpolar aromatic compounds to four surface soils of eastern China. *Environ. Pollut.* **2008,** 156(3), 1053-1060

(159) Shirzadi, A.; Simpson, M. J.; Kumar, R.; Baer, A. J.; Xu, Y.; Simpson, A. J., Molecular interactions of pesticides at the soil-water interface. *Environ. Sci. Technol.* **2008,** 42(15), 5514-5520.

(160) Xing, B. S.; Pignatello, J. J., Dual-mode sorption of low-polarity compounds in glassy poly(vinyl chloride) and soil organic matter. *Environ. Sci. Technol.* **1997,** 31(3), 792-799.

(161) Schlautman, M. A.; Morgan, J. J., Effects of aqueous chemistry on the binding of polycyclic aromatic-hydrocarbons by dissolved humic materials. *Environ. Sci. Technol.* **1993,** 27(5), 961-969.

(162) Smejkalova, D.; Piccolo, A., Host-guest interactions between 2,4-dichlorophenol and humic substances As evaluated by 1H NMR relaxation and diffusion ordered spectroscopy. *Environ. Sci. Technol.* **2008,** 42(22), 8440–8445.

(163) Viel, S.; Mannina, L.; Segre, A., Detection of a pi-pi complex by diffusion-ordered spectroscopy (DOSY). *Tetrahedron Lett.* **2002,** 43(14), 2515-2519.

(164) McDermott, M. T.; McCreery, R. L., Scanning tunneling microscopy of ordered graphite and glassy carbon surfaces: electronic control of quinone adsorption. *Langmuir* **1994,** 10(11), 4307-4314.

(165) Zhu, D. Q.; Pignatello, J. J., Characterization of aromatic compound sorptive interactions with black carbon (charcoal) assisted by Graphite as a Model. *Environ. Sci. Technol.* **2005,** 35(7), 2033-2041

(166) Zhu, D. Q.; Kwon, S.; Pignatello, J. J., Adsorption of single-ring organic compounds to wood charcoals prepared under different thermochemical conditions. *Environ. Sci. Technol.* **2005,** 39(11), 3990-3998.

(167) Sander, M.; Pignatello, J. J., Characterization of charcoal adsorption sites for aromatic compounds: Insights drawn from single-solute and Bi-solute competitive experiments. *Environ. Sci. Technol.* **2005,** 39(6), 1606-1615.

(168) Hawthorne, S. B.; Poppendieck, D. G.; Grabanski, C. B.; Loehr, R. C., Comparing PAH availability from manufactured gas plant soils and sediments with chemical and biological tests. 1. PAH release during water desorption and supercritical carbon dioxide extraction. *Environ. Sci. Technol.* **2002,** 36(22), 4795-4803.

(169) Hong, L.; Ghosh, U.; Mahajan, T.; Zare, R. N.; Luthy, R. G., PAH sorption mechanism and partitioning behavior in lampblack-impacted soils from former oil-gas plant sites. *Environ. Sci. Technol.* **2003,** 37(16), 3625-3634.

(170) Kubicki, J. D., Molecular simulations of benzene and PAH interactions with soot. *Environ. Sci. Technol.* **2006,** 40(7), 2298-2303.

(171) Wang, X. L.; Sato, T.; Xing, B. S., Competitive sorption of pyrene on wood chars. *Environ. Sci. Technol.* **2006,** 40(10), 3267-3272.

(172) Lin, D.; Xing, B., Tannic acid adsorption and its role for stabilizing carbon nanotube suspensions. *Environ. Sci. Technol.* **2008,** 42(16), 5917-5923.

(173) Woods, L. M.; Badescu, S. C.; Reinecke, T. L., Adsorption of simple benzene derivatives on carbon nanotubes. *Phys. Rev. B: Condens. Matter* **2007,** 75(15), 155415.

(174) Islam, M. F.; Rojas, E.; Bergey, D. M.; Johnson, A. T.; Yodh, A. G., High weight fraction surfactant solubilization of single-wall carbon nanotubes in water. *Nano Lett*. **2003,** 3(2), 269-273.

(175) Wang, Z. W.; Liu, C. L.; Liu, Z. G.; Xiang, H.; Li, Z.; Gong, Q. H., pi-pi interaction enhancement on the ultrafast third-order optical nonlinearity of carbon nanotubes/polymer composites. *Chem. Phys. Lett*. **2005,** 407(1-3), 35-39.

(176) Zhao, J. J.; Lu, J. P.; Han, J.; Yang, C. K., Noncovalent functionalization of carbon nanotubes by aromatic organic molecules. *Appl. Phys. Lett*. **2003,** 82(21), 3746-3748.

(177) Jorgensen, W. L.; Severance, D. L., Aromatic aromatic interactions - free-energy profiles for the benzene dimer in water, chloroform, and liquid benzene. *J. Am. Chem. Soc*. **1990,** 112(12), 4768-4774.

(178) Qu, X.; Xiao, L.; Zhu, D. Q., Site-specific adsorption of 1,3-dinitrobenzene to bacterial surfaces: a mechanism of n–{pi} electron-donor-acceptor interactions. *J. Environ. Qual*. **2008,** 37, 824-829.

(179) Mooibroek, T. J.; Gamez, P.; Reedijk, J., Lone pair–interactions: a new supramolecular bond? *CrystEngComm* **2008,** 10, 1501 - 1515.

(180) Brandl, M.; Weiss, M. S.; Jabs, A.; Sühnel, J.; Hilgenfeld, R., Ch···π-interactions in proteins. *J. Mol. Biol*. **2001,** 307, 357-377.

(181) Tsuzuki, S.; Honda, K.; Uchimaru, T.; Mikami, M.; Tanabe, K., Origin of the attraction and directionality of the NH/pi interaction: Comparison with OH/pi and CH/pi interactions. *J. Am. Chem. Soc*. **2000,** 122(46), 11450-11458.

(182) Lee, J. Y.; Lee, S. J.; Choi, H. S.; Cho, S. J.; Kim, K. S.; Ha, T. K., Ab-initio study of the complexation of benzene with ammonium cations. *Chem. Phys. Lett*. **1995,** 232(1-2), 67-71.

(183) Aschi, M.; Mazza, F.; Di Nola, A., Cation-pi interactions between ammonium ion and aromatic rings: an energy decomposition study. *Journal of Molecular Structure-THEOCHEM* **2002,** 587, 177-188.

(184) Emsley, J., Very strong hydrogen-bonding. *Chem. Soc. Rev*. **1980,** 9(1), 91-124.

(185) Feyereisen, M. W.; Feller, D.; Dixon, D. A., Hydrogen bond energy of the water dimer. *J. Phys. Chem*. **1996,** 100(8), 2993-2997.

(186) Sutton, R.; Sposito, G., Molecular structure in soil humic substances: The new view. *Environ. Sci. Technol*. **2005,** 39(23), 9009-9015.

(187) Chenu, C.; Plante, A. F., Clay-sized organo-mineral complexes in a cultivation chronosequence: revisiting the concept of the 'primary organo-mineral complex'. *Eur. J. Soil Sci*. **2006,** 57(4), 596-607.

(188) Christensen, B. T., Physical fractionation of soil and structural and functional complexity in organic matter turnover. *Eur. J. Soil Sci*. **2001,** 52(3), 345-353.

(189) Lehmann, J.; Kinyangi, J.; Solomon, D., Organic matter stabilization in soil microaggregates: implications from spatial heterogeneity of organic carbon contents and carbon forms. *Biogeochemistry* **2007,** 85(1), 45-57.

(190) Mikutta, R.; Schaumann, G.; Gildemeister, D.; Bonneville, S.; Kramer, M. G.; Chorover, J.; Chadwick, O. A.; Guggenberger, G., Biogeochemistry of mineral-organic associations across a long-term mineralogical soil gradient (0.3-4100 kyr), Hawaiian Islands. *Geochim. Cosmochim. Acta* **2009,** in press, doi: 10.1016/j.gca.2008.12.028.

(191) Kinyangi, J.; Solomon, D.; Liang, B.; Lerotic, M.; Wirick, S.; Lehmann, J., Nanoscale biogeocomplexity of the organomineral assemblage in soil: Application of STXM microscopy and C 1s-NEXAFS spectroscopy. *Soil Sci. Soc. Am. J.* **2006,** 70(5), 1708-1718.

(192) Hundal, L. S.; Thompson, M. L., Soil aggregation as a source of variation in sorption isotherms of hydrophobic organic compounds. *Soil Sci.* **2006,** 171(5), 355-363.

(193) Zhang, Y.; Zhu, D.; Yu, H., Sorption of aromatic compounds to clay mineral and model humic substance-clay complex: Effects of solute structure and exchangeable cation. *J. Environ. Qual.* **2008,** 37(3), 817-823.

(194) Zimmerman, A. R., Abiotic and Microbial Oxidation of Laboratory-Produced Black Carbon (Biochar). *Environ. Sci. Technol.* **2010,** in print, available online at http://pubs.acs.org/journals/esthag/index_news.html.

(195) Atkins, P. W.; de Paula, J., *Physical Chemistry*. 8th ed.; Oxford University Press: Oxford, 2006.

(196) Liang, W. Y., Excitons. *Phys. Edu.* **1970,** 5, 226-228.

(197) Ahuja, R.; Bruhwiler, P.; Wills, J.; Johansson, B.; Martensson, N.; Eriksson, O., Theoretical and experimental study of the graphite 1s x-ray absorption edges. *Phys Rev B* **1996,** 54(20), 14396-14404.

(198) Batson, P., Carbon-1s near-edge-absorption fine-structure in graphite. *Phys. Rev. A* **1993,** 48(4), 2608-2610.

(199) Bruhwiler, P.; Maxwell, A.; Puglia, C.; Nilsson, A.; Anderson, S.; Martensson, N., Pi-asterisk and sigma-asterisk excitations in C-1s absorption of graphite. *Phys. Rev. Lett.* **1995,** 74(4), 614-617.

(200) Coffman, F.; Cao, R.; Pianetta, P.; Kapoor, S.; Kelly, M.; Terminello, L., Near-edge x-ray absorption of carbon materials for determining bond hybridization in mixed sp2/sp3 bonded materials. *Appl. Phys. Lett.* **1996,** 69(4), 568-570.

(201) Abbas, M.; Wu, Z.; Zhong, J.; Ibrahim, K.; Fiori, A.; Orlanducci, S.; Sessa, V.; Terranova, M.; Davoli, I., X-ray absorption and photoelectron spectroscopy studies on graphite and single-walled carbon nanotubes: Oxygen effect. *Appl. Phys. Lett.* **2005,** 87(5), 051923.

(202) Pong, W.; Yueh, C.; Chang, Y.; Tsai, M.; Chang, Y.; Chen, Y.; Lee, J.; Wei, S.; Wen, C.; Chen, L.; Chen, K.; Lin, I.; Cheng, H., X-ray absorption studies of carbon-related materials. *J. Synchrotron Rad.* **2001,** 8, 145-149.

(203) Braun, A.; Mun, B. S.; Huggins, F. E.; Huffman, G. P., Carbon speciation of diesel exhaust and urban particulate matter NIST standard reference materials with C(1s) NEXAFS spectroscopy. *Environ. Sci. Technol.* **2007,** 41(1), 173-178.

(204) Hopkins, R. J.; Tivanski, A. V.; Marten, B. D.; Gilles, M. K., Chemical bonding and structure of black carbon reference materials and individual carbonaceous atmospheric aerosols. *J. Aerosol Sci.* **2007,** 38(6), 573-591.

(205) Guo, Y.; Bustin, R. M., FTIR spectroscopy and reflectance of modern charcoals and fungal decayed woods: implications for studies of inertinite in coals. *Int. J. Coal Geol.* **1998,** 37(1-2), 29-53.

(206) Lin-Vien, D.; Colthup, N. B.; Fateley, W. G.; Grassell, J. G., *The handbook of infrared and raman characteristic frequencies of organic molecules*. Academic Press, Inc.: San Diego, CA, 1991.

(207) van der Marel, H. M.; Beutelspacher, H., *Atlas of infrared spectroscopy of clay minerals and their admixtures*. Elsevier Scientific Pub.: New York, 1976.

(208) Mochidzuki, K.; Soutric, F.; Tadokoro, K.; Antal, M. J.; Toth, M.; Zelei, B.; Varhegyi, G., Electrical and physical properties of carbonized charcoals. *Ind. Eng. Chem. Res.* **2003,** 42(21), 5140-5151.

(209) Friel, J. J. M., S.; Follweiler, D. M., Electron optical and IR spectroscopic investigation of coal carbonization. In *Coal and coal products: Analytical characterization techniques*, Fuller, E. L., Ed. American Chemical Society: Washington, DC, 1982; p 294.

(210) Pretsch, E.; Bühlmann, P.; Badertscher, M., *Structure Determination of Organic Compounds*. Springer-Verlag: Berlin, 2009.

(211) Smith, D. M.; Chughtai, A. R., The surface-structure and reactivity of black carbon. *Colloid Surface A* **1995,** 105(1), 47-77.

(212) Chen, B.; Johnson, E.; Chefetz, B.; Zhu, L.; Xing, B., Sorption of polar and nonpolar aromatic organic contaminants by plant cuticular materials: Role of polarity and accessibility. *Environ. Sci. Technol.* **2005,** 39(16), 6138-6146.

(213) Koch, A.; Krzton, A.; Finqueneisel, G.; Heintz, O.; Weber, J.; Zimny, T., A study of carbonaceous char oxidation in air by semi-quantitative FTIR spectroscopy. *Fuel* **1998,** 77(6), 563-569.

(214) Pradhan, B.; Sandle, N., Effect of different oxidizing agent treatments on the surface properties of activated carbons. *Carbon* **1999,** 37(8), 1323-1332.

(215) Bustin, R.; Guo, Y., Abrupt changes (jumps) in reflectance values and chemical compositions of artificial charcoals and inertinite in coals. *Int. J. Coal Geol.* **1999,** 38(3-4), 237-260.

(216) Haberhauer, G.; Rafferty, B.; Strebl, F.; Gerzabek, M., Comparison of the composition of forest soil litter derived from three different sites at various decompositional stages using FTIR spectroscopy. *Geoderma* **1998,** 83(3-4), 331-342.

(217) López-Pasquali, C. E.; Herrera, H., Pyrolysis of lignin and IR analysis of residues. *Thermochim. Acta* **1997,** 293(1-2), 39-46.

(218) Labbe, N.; Harper, D.; Rials, T., Chemical structure of wood charcoal by infrared spectroscopy and multivariate analysis. *J. Agric. Food Chem.* **2006,** 54(10), 3492-3497.

(219) Lehmann, J.; Liang, B. Q.; Solomon, D. H.; Lerotic, M.; Luizao, F.; Kinyangi, J.; Schafer, T.; Wirick, S.; Jacobsen, C., Near-edge X-ray absorption fine structure (NEXAFS) spectroscopy for mapping nano-scale distribution of organic carbon forms in soil: Application to black carbon particles. *Global Biogeochem. Cycles* **2005,** 19(1), GB1013, doi:10.1029/2004GB002435.

(220) Brandes, J. A.; Lee, C.; Wakeham, S.; Peterson, M.; Jacobson, C.; Wirick, S.; Cody, G., Examining marine particulate organic matter at sub-micron scales using scanning transmission X-ray microscopy and carbon X-ray absorption near edge structure spectroscopy. *Mar. Chem.* **2004,** 92(1-4), 107-121.

(221) Myneni, S. C. B. In *Applications of synchrotron radiation in low-temperature geochemistry and environmental sciences*, Reviews in Mineralogy and Geochemistry, Jan 1, 2002; Fenter, P. A.; Rivers, M. L.; Sturchio, N. C.; Sutton, S. R., Eds. Mineralogical Society of America: 2002; pp 485-579.

(222) Zhong, J.; Song, L.; Yan, D.; Wu, Z.; Wang, C.; Xie, S.; Qian, H., A XANES characterization of structural defects in single-walled carbon nanotubes. *Radiat. Phys. Chem.* **2006,** 75(11), 1861-1865.

6 Appendix

6.1 1s-π* exciton phenomenon (NEXAFS)

If electronic excitation of an ion in a crystal is considered, the excitation corresponds to the removal of an electron from one orbital of a molecule and its elevation to an orbital of higher energy, the excited state of the molecule can be envisaged as the coexistence of an electron and a hole. Extensive highly conjugated sp^2-bonded carbon domains such as graphene permit the electron and the hole to migrate. This mobile excitation is referred to as an exciton (*195, 196*). 1s-σ* exciton signals were found in NEXAFS spectra of graphite (*197-200*), carbon nanotubes (*71, 201, 202*) and carbonaceous particulate matter (*52, 203, 204*).

6.2 Fourier transform infrared spectroscopy

The evolution of FT-IR spectra of wood and grass chars as a function of charring temperature is shown in Fig. 1. No FT-IR detectable chemical changes occur as plant material is heated to 100 and 200˚C. More noteworthy changes occur at 300˚C, particularly for grass char. After heating to 300˚C, there were stronger C=O and C=C stretching vibrations at 1700 and 1600 cm^{-1} indicating the formation of ketones, anhydrides, esters, and carboxylic C as well as aromatic components (*42, 205*). At the same time the absorbance of the dominant C-O stretch at 1030 cm^{-1} associated with cellulose, hemicellulose, and lignin slightly decreased.

Heating to 400˚C results in more substantial chemical transformations. Bands due to hydrogen bonded O-H stretching (3200-3500 cm^{-1}) of water molecules loose

intensity. Absorption of the aliphatic C-H stretching (2935 and 2885 cm^{-1}) decreases slightly but sustains a strong presence indicative of heat-resistant aliphatic structures. Greater aromatic C=C stretching vibrations (1600 cm^{-1}) become the dominant feature for both wood and grass chars. Further evidence for aromatic C is provided by the appearance of three bands between 885 and 750 cm^{-1} (out-of-plane deformations of aromatic C-H (*205, 206*)). The signals near 815 and 750 cm^{-1} may indicate O-substitution of quinone and furan-like structures (*207*). Specifically, the presence of ring C-H stretch bands at 3200 cm^{-1} suggests five-membered N/O-heterocycles such as furan and pyrrole (*206*).

The intensity of bands reflecting undecomposed cellulosic and ligneous C decline (most obvious at 1030 cm^{-1}) at 400˚C. Conversely, both wood and char spectra show evidence for lignin- and cellulose-derived transformation products. Ligneous products are reflected in more prominent peaks at 1440 (C=O stretching of ketones) and 1375 cm^{-1} (O-H bending of phenols). Cellulose-derived products in wood are suggested by bands at 1185 and 1270 cm^{-1}, corresponding to C-O stretching of pyranone rings and guaiacyl monomers, respectively. Signals at 1180-1030 cm^{-1} in grass chars may arise from the C-H deformation of cellulose-derived substituted aromatics (*75*).

Between 500 and 700˚C, all features related to water, oxygenated substituents, aliphatic C, and the aromatic C=C stretch progressively decline. Two exceptions from this trend involving aromatic components are absorption by C-H stretching (3050 cm^{-1}) and C-H out-of-plane vibrations (885-750 cm^{-1}). An increase of intensity at 885-752 relative to 1650-1500 cm^{-1} indicates a larger degree of

condensation (*205*). Heating from 400 to 700˚C progressively increases this ratio, confirming that smaller (substituted) aromatic units condense into larger sheets. At 700˚C, any residual C functionalities diminish and grass and wood char spectra become very similar. Both resemble closely FT-IR spectra of pure graphite (as displayed, e.g., in (*208*).

The fact that the baseline of both wood and char is progressively shifted upward with increasing temperature is a common phenomenon in spectra of carbonized materials (*209*). As a result of increasing diffuse absorption of the sample, the upward shift is assigned to low-energy electron excitations of condensed aromatic structures (*208*).

To summarize, FT-IR spectra show (i) dehydration of cellulosic and ligneous components starting at 300˚C, (ii) a strong presence of (heterocyclic) aromatic C and lignin/cellulose-derived transformation products at 400˚C, and (iii) an increasing degree of condensation at charring temperatures of 500˚C and beyond.

Table A-1: Assignment of characteristic vibrations to individual peaks in wood and grass char ATR FT-IR spectra.

Wavenumber [cm^{-1}]	Characteristic vibrations	Functionality
3665	'free' O-H stretching	alcoholic and phenolic -OH, not hydrogen bonded (*210*) (*211*)
3200-3500	O-H stretching	water, H-bonded hydroxyl (-OH) groups (*210*) (*211*)
3200	C-H stetching	5-membered N/O-heterocyclic C (e.g., furans and pyrroles) (*206*)
3050	C-H stretching	substituted aromatic C (*206*)
2935	asymmetric C-H stretching	aliphatic CH_x (*212*)
2885	symmetric C-H stretching	aliphatic CH_x (*212*)
1740-1700	C=O stretching	mainly carboxyl (*42*); traces of aldehydes, ketones and esters (*213*) (*214*)
1600	C=C stretching	aromatic components (*42*) (*215, 216*)
	C=O stretching	C=O of conjugated ketons and quinones (*42*) (*215, 216*)
1510	C=C stretching	aromatic skeletal vibrations, indicative of lignin (*215, 216*) (*217*)
1440	C=C stretching	aromatic C, indicative of lignin, appears when bound to unsaturated group (*215, 216*) (*217*)
	α-C-H_2 bending	aliphatic -CH_2 deformations (*211*), associated with lignin and carbohydrates (*218*)
1375	O-H bending	in plane bending of phenolic -OH (*219*), related to ligneous syringyl units (*217*)
	α-C-H_3 bending	aliphatic -CH_3 deformations (*42*) (*215, 216*)
1270-1250	C-O stretching	C-O-C groups and aryl ethers (*211*) (*42*); phenolic C-O indicative of guaiacyl units associated with lignin (*217*) (*72*)
1185-1160	(asymmetric) "	C-O-C ester groups in cellulose and hemicellulose (*75*) (*218*)
1110	(symmetric) "	C-O-C stretching vibrations in cellulose and hemicellulose [j]; aliphatic -OH (*210*)
1030	"	acid derivatives, aliphatic C-O-C, and -OH representative of oxygenated functional groups of cellulose and hemicellulose (*214*) (*218*); methoxy groups of lignins (*72*)
1200-1000	C-H deformation	vibrations typical for substituted aromatics (*75*)
885, 815, 750	C-H bending	aromatic CH out-of-plane deformation (*215, 216*); less substituted rings appear at lower wavenumbers (*210*)

Table A-2: Peak assignments for C forms obtained from C (1s) NEXAFS

Photon energy [eV]	Transition	C form	Functionality
284.3	1s-π*	C=C	quinone (*64*)
285.3	1s-π*	C=C	unsaturated/aromatic (*62*); graphitic (*197, 198*)
286.4	1s-π*	C=O	ketone, carbonyl substituted aromatic (*67, 68, 203*)
287.1 - 287.3	1s-3p/σ*	C-H	aliphatic (*63, 67, 220*)
	1s-π*	C-OH	phenol -OH (*63*); aliphatic -OH (*221*)
		C-OR	O-substituted aromatic C (*64*) (*55*)
288.6	1s-π*	C=O	carboxyl (*67*); aldehyde (*63*)
289.2 - 289.3	1s-3p/σ*	C-O	alcohols (*67*) (*220*)
		C-O	secondary alcohols in polysaccharides, hemicellulose and cellulose, propyl side chains and methoxyl carbons of lignin (*55*)
291.2 - 291.6	1s-σ* exciton	C-C	extensive conjugated aromatic sheets (*65, 66, 199, 200*)
292 - 295	1s-σ*	C-C	aromatic (*63, 198*); long-range order (*222*)